Universiteit Utrecht

A Monte-Carlo Approach to Anisotropic Flow in Heavy-Ion Collisions

-

Lennart van Doremalen

January 16, 2013

Bachelor Thesis

Report number: UU(SAP) 13-1

Supervisors:
Prof. Dr. Raimond Snellings
MSc. Redmer Bertens

Utrecht University
Faculty of Science/Department of Physics and Astronomy
Institute for Subatomic Physics
Buys Ballot laboratory
PO BOX 80 000, 3508 TA Utrecht, The Netherlands

Prologue

The main purpose of this thesis, as will be explained in later chapters, is to look at the anisotropic flow of (composite) particles, like the phi meson, that are formed during the hadronization period directly after the creation of a Quark-Gluon Plasma (QGP) in order to learn more about the properties of the QGP. In order to get accurate anisotropic flow estimates for the different particle species that are detected after their creation in heavy-ion collisions new analysis methods have been developed. The research in this thesis has contributed to the validation of these analysis methods.

Contents

Chapter 1
Introduction

After the discovery of the divisibility of the atom, by J.J. Thompson in the year 1897, experiments were conceived of ever increasing size to probe the subatomic world and see how far down the rabbit hole we can go. Through these experiments we have gained an understanding of the buildings blocks of the atom and the forces that keep these constituents together. The particles that make up the atomic nucleus are called protons and neutrons, both of which have their own building blocks we call quarks that are kept together in a confined space by the strong force. This strong force and its interaction with all quarks is described by Quantum Chromo Dynamics (QCD).

It is expected that for a very short duration after the Big Bang quarks and the particles that carry the strong force, called gluons, formed a primordial state of matter called a Quark-Gluon Plasma (QGP). In order to understand why the QGP is expected to form and what properties it is expected to have we will first introduce the basic concepts of Quantum Chromo Dynamics in section 1 of this chapter. In section 2 we will review our current understanding of the QGP and in section 3 we will look at how we can create and learn more about the QGP.

1.1 - Quantum Chromo Dynamics

As you know protons and electrons, which are described by Quantum Electrodynamics (QED), carry a positive and a negative electric charge respectively. When a proton and electron are close together their charges cancel out so that they become electrically neutral. Quarks carry a charge we call colour in a similar way as protons and electrons carry their electric charge. A quark that has a colour charge "Red" can combine with a quark that has the colour charge "anti-Red" so that they become colour neutral. Unlike protons and electrons, quarks can also be colour neutral when in a pair of three quarks. In order to describe this we say that a quark can have three different colours (Red, Green or Blue) or one of three anti-colours (anti-Red, anti-Green or anti-Blue).

The gluon is the QCD's counterpart of the photon that carries the electromagnetic force between electrically charged particles. Just like the quark, the gluon is different in several aspects to its electromagnetic equivalent. The gluon caries a positive and a negative colour charge in contrast to the photon that does not carry any electric charge. Because gluons have two colour charges they are able to change the colour charge of a quark if this quark has a colour charge opposite to one of the colour charges of the gluon. Another important property of the gluon is its ability to interact with other gluons. Photons can only interact with particles that have an electric charge, since they don't have an electric charge themselves, they do not interact with each other. The fact that the gluon has a colour charge makes it possible for the gluon to interact with other gluons. It also gives rise to some fundamental effects that lie at the basis of Quantum Chromo Dynamics.

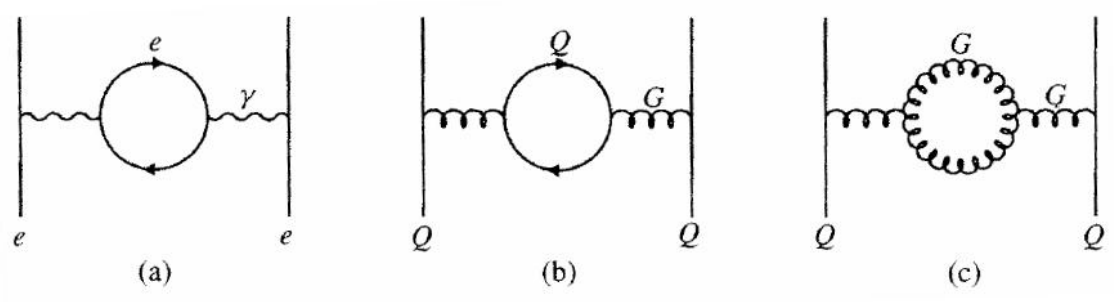

Figure 1.1: "Diagrams involving loops (vacuum polarisation effects) (a) in QED, where loops contain fermions only, (b) in QCD for a loop containing quarks and (c) in QCD for a gluon loop, involving gluon-gluon coupling, absent in QED." [5]

Asymptotic freedom – When we have an electrically charged particle in a dielectric medium it will induce a shielding effect that screens (hides) a fraction of the charge of the particle. Even in vacuum an electrically charged particle will experience a screening effect due to the creation of virtual charge anti-charge pairs in the vacuum. Quarks experience the same effect for their colour charge but they are also affected by an anti-screening effect. When two (or more) quarks are separated virtual quarks, virtual transverse gluons and virtual longitudinal gluons are created (see fig. 1.1) between the separated quarks. While the virtual quarks and transverse gluons cause a slight screening effect of the colour charges of the quarks, the strong force between the quarks is enhanced more by the virtual longitudinal gluons. The strength of this anti-screening is inversely dependant on the amount of momentum transfer between the quarks. This means that the further two separated quarks are away from each other the more strongly they are attracted to one another. The strong force can become so strong between the quarks that at some distance it is more energetically favourable to create a new quark anti-quark pair that recombines with original quarks. The anti-screening effects are called asymptotic freedom because the quarks are 'free' from the effects of the strong force in the limit of infinite momentum transfer with other particles with colour charge.

Confinement – Confinement is the experimental observation that quarks and anti-quarks are only observed in combined colour neutral states. Examples are baryons, which consists of three quarks like the proton and the neutron, and mesons, which consists of two quarks like the phi-meson. Individual quarks, anti-quarks or other non-neutral colour states have never been found. This can be attributed to the effects of asymptotic freedom mentioned above.

1.2 – Quark-Gluon Plasma

As the temperature of a system increases so does the momentum transfer between the particles in the system. Since the properties of asymptotic freedom tell us that the strength of the strong force decreases for higher momentum transfer it has been

expected for several decades that quarks and gluons can form a deconfined, weakly interacting, gas at a given temperature and pressure. In this gas thermal fluctuations (in the gauge fields) can cause a dominant screening over anti-screening of the colour charge, much like the electric charge of electrically charged particles in a plasma are screened. Therefore the state of matter consisting of deconfined quarks and gluons has been dubbed a Quark-gluon Plasma by Edward Shuryak in 1978.

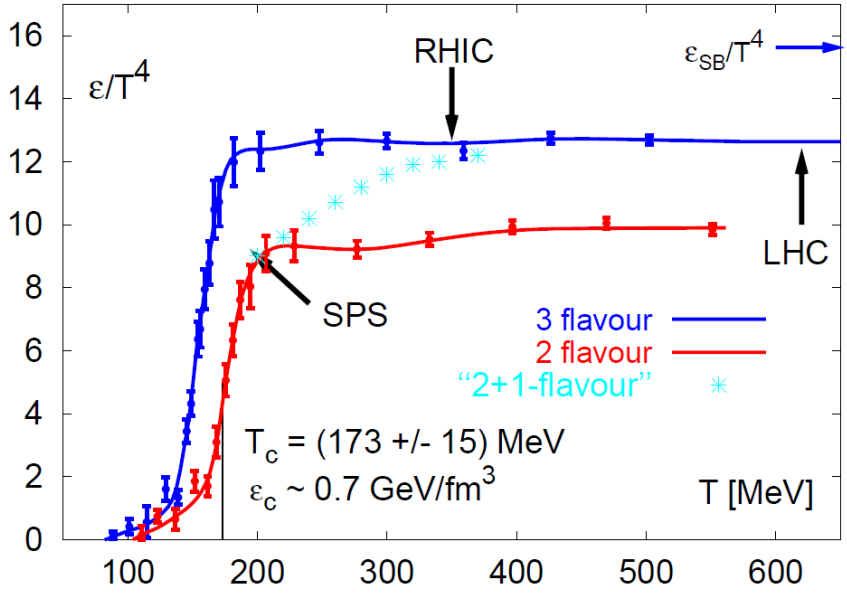

Figure 1.2: The graph shows the sudden increase in energy density for different sorts of QCD matter for temperatures above a given critical temperature. The graphs are based on Lattice QCD, in which the field equations of QCD are solved numerically on a discrete space-time grid. The black arrows indicate the temperature range of the detector and the blue arrow indicates the Stefan Boltzamnn limit of the energy density. [2, 7, 10]

In order to create a QGP we need to create a situation in which the quarks of a composite particle can exchange enough momentum to get in a deconfined state. By accelerating two heavy ions (like the atomic nuclei of two lead atoms), in a particle accelerator, to speeds close to the speed of light and letting them collide in the centre of a detector, we create a very hot and very dense system of quarks and gluons. The quarks, in this system, are forced to exchange their momentum giving them a short window of opportunity to form a QGP before being thrust outwards by the sheer amount of pressure. The transition temperature and energy density, for quarks to deconfine and form a QGP, are predicted to be approximately 175 MeV and 0.7 GeV/fm^3 respectively (see fig. 1.2).

The size of the QGP that is formed in a heavy-ion collision, and thereby the amount of quarks and gluons that are involved, depends on the centrality of the collision and the distribution of the quarks in the nuclei. In general most heavy-ion

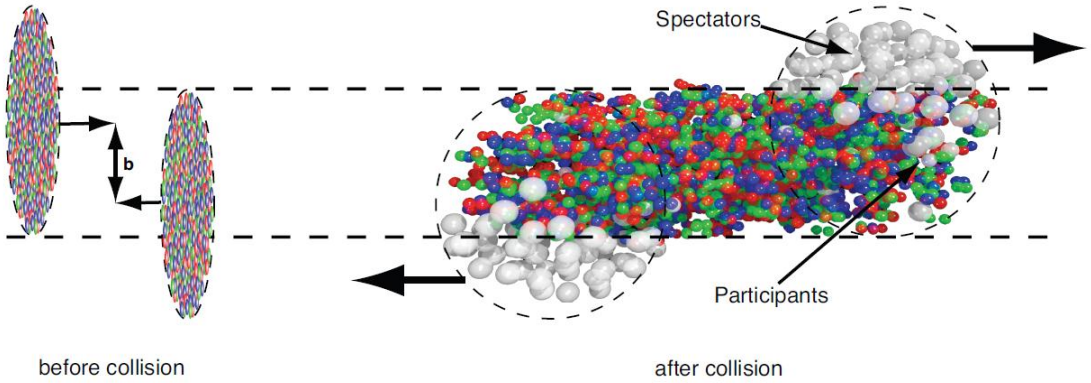

Figure 1.3: A relativistic heavy ion collision. - Left: before the collision both nuclei are Lorentz contracted and transversely separated by an impact parameter b. - Right: the particles in the overlapping regions interact with each other while the non-participating particles, called spectators, remain unaffected. [10]

collisions will not be head-on collisions. Only a part of the nuclei will overlap during the collision and only the quarks that are present in the overlapping regions will participate in the collision (see fig. 1.3).

So far experiments have been unable to confirm or deny the creation of a QGP in heavy ion collisions even though the required temperature and energy density for the formation of a QGP are met. The results of these experiments do show however that the formed matter behaves not as a weakly interacting gas but as an almost perfect liquid which has a high density and a very low kinematic viscosity. [8]

1.3 – Probing the Quark-Gluon Plasma

The main goals in relativistic heavy-ion collisions (H.I.C.) are to create a QGP and to study its properties. [9] In order to understand these properties we can look at observables from H.I.C. that tell us more about the properties of the matter produced during H.I.C.

The observable we look at in this thesis is elliptic flow as a function of transverse momentum[1]. In order to introduce the concept of elliptic flow we will first look at the basic concepts of flow and anisotropic flow. Then we will look at elliptic flow and how it can be used to learn more about heavy-ion collisions. Mathematically flow can be described by relativistic hydrodynamics. Relativistic hydrodynamics has proved to be the most successful theory in describing experimental anisotropic flow data collected at collider energies so far [1]. A detailed study on the description of flow by the use of relativistic hydrodynamics is given in [9].

[1] We look at transverse momentum instead of the total particle momentum because the longitudinal momentum may be the result of a difference in the momentum of the colliding particles.

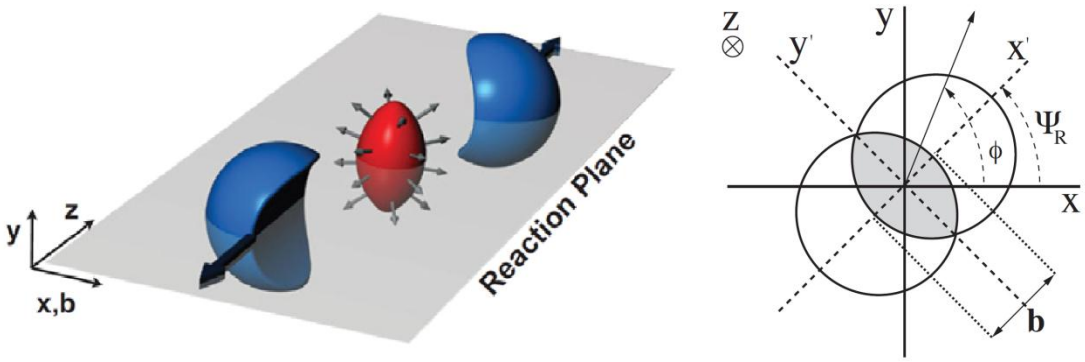

Figure 1.4 - Left: After a non-central collision, the particles that participated in the collision have an almond like shape that will expand outward while the nucleus remnants continue in the same path of flight. The plane spanned by the vector of the beam direction and the impact parameter **b** (the vector connecting the two centres of the colliding nuclei) is called the reaction plane. - Right: A cross-section of the collision in the left picture, showing the angle from the lab frame to the reaction plane and the azimuthal angle for a given particle. [2, 10]

1.3.1 – Flow

Flow is the collective motion of a volume of matter due to a density gradient. The interactions of the particles in the volume create a pressure that results in an expansion in the direction of lower density. Since the density of collided heavy ions is a lot higher than the near-vacuum in which they are, the formed matter will experience a radial flow outwards called collective flow. This collective flow is dependent on the strength of the interactions between the particles that make up the volume of matter.

1.3.2 – Anisotropic flow

As stated in the previous section, most collisions won't be head-on collisions but collisions that only overlap partly. This non-centrality results in an almond shaped volume of particles as can been seen in figure 1.4. The anisotropy of the volume results in an anisotropic momentum space. We can quantify the anisotropy in the momentum space with flow harmonics v_n as coefficients of the Fourier expansion of the azimuthal dependence of the Lorentz invariant yield of particles relative to the reaction plane [1, 12]:

$$E\frac{d^3N}{d^3p} = \frac{1}{2\pi}\frac{d^2N}{p_t\,dp_t\,dy}\left(1 + \sum_{n=1}^{\infty} 2v_n \cos\big(n(\phi - \Psi_R)\big)\right) \tag{1.1}$$

Here E is the energy of the particle, p is its momentum, p_t is its transverse momentum, ϕ is its azimuthal angle (see fig. 1.4), y is its rapidity and Ψ_R is the

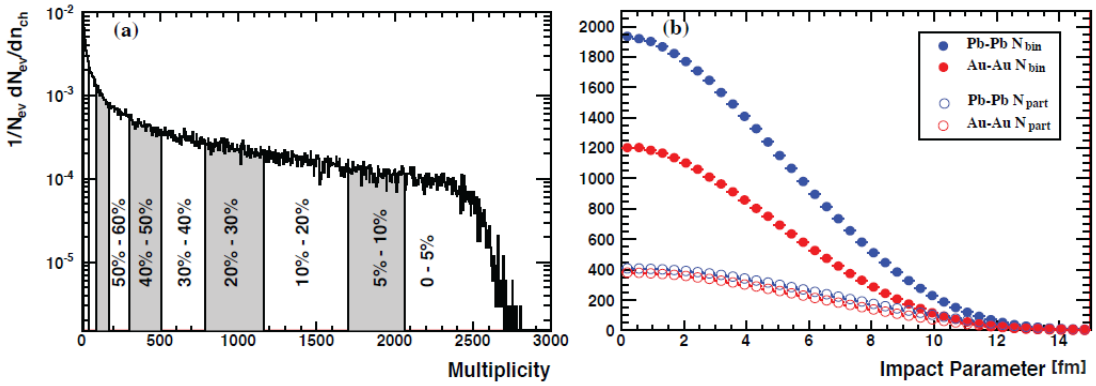

Figure 1.5 - Left: The amount of produced charged particles (multiplicity) in lead-lead collisions at $\sqrt{s_{NN}} = 2.76$ TeV as a function of the centrality of the collision. - Right: The number of participating nucleons N_{part} and binary collisionsN_{bin} versus the impact parameter for lead-lead and gold-gold collisions at $\sqrt{s_{NN}} = 2.76$ and 0.2 TeV respectively. [10]

reaction plane angle of the event. Rapidity is a quantity that describes the velocity of the particle in a way that is Lorentz-invariant. For ultra-relativistic particles this is equal to pseudo-rapidity, which can be derived from the polar angle θ between the particle and the beam direction. The pseudo-rapidity is given by [4]:

$$\eta = -\log\left(\tan\frac{\theta}{2}\right) = \frac{1}{2}\log\left(\frac{|p| + p_l}{|p| - p_l}\right) \cong y = \frac{1}{2}\log\left(\frac{E + p_l}{E - p_l}\right) \tag{1.2}$$

Where p_l is the longitudinal momentum of the particle. The v_n coefficients of equation 1.1 are given by [4, 11]:

$$v_n(p_t, y) = \langle\cos\big(n(\phi - \Psi_R)\big)\rangle \tag{1.3}$$

The v_1 coefficient is called directed flow and the v_2 coefficient is called elliptic flow. In order to measure v_n we need to know the azimuthal angles ϕ and Ψ_R. We can measure ϕ directly but we cannot measure Ψ_R directly. In order to get the value of v_n we need another way to measure v_n. This can be done by several ways, which are described in chapter 2.1 for the case of elliptic flow.

1.3.3 – Elliptic flow

Of all the v_n coefficients, the v_2 coefficient is expected to be the dominant harmonic in non-central collisions due to the initial elliptic collision geometry. [1] This geometry is dependent of the centrality of the collision, which results in a correlation between the collision centrality and elliptic flow. Since the number of participating nucleons, in a collision, is also dependent on the type of nuclei used in the collision, the elliptic flow will be affected by this (see fig. 1.5). [10]
The dependence of elliptic flow on the transverse momentum is dependent on several fundamental properties of interest we can look at if we keep the other factors constant.

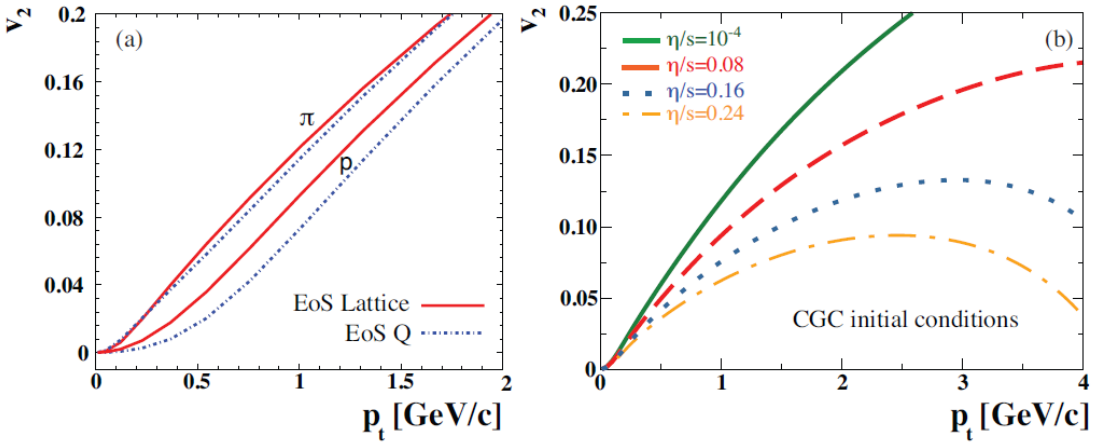

Figure 1.6: - Left: The predicted v_2 as a function of p_t for a Pion and a Proton for different Equations of State. - Right: This graph shows the effect of possible values for the shear viscosity ($\boldsymbol{\eta/s}$) on the p_t dependence of v_2. [10]

By measuring v_2 as a function of transverse momentum we can discover which theoretical predictions are closest for some of these fundamental properties, like the Equation of state, Shear Viscosity (see fig. 1.6) and the speed of sound in the produced matter. [10]

These predictions are dependent on fundamental assumptions on the parton distribution inside the nucleus of an atom. Two models on this distribution, the Glauber and the Colour Glass Condensate (CGC) model, are described below.

Glauber: The Glauber model is a Monte Carlo model that uses a quantum-mechanical probability function to distribute a number of nucleons stochastically in two simulated nuclei. These nuclei are considered to be Lorentz contracted and transversely separated by an impact parameter **b** (see fig. 1.3). The collision is treated as a sum of proton-proton collisions, which provides the data to relate the H.I.C. observables with the initial condition of the formed matter. [4]

Colour Glass Condensate: The CGC is a two dimensional model of a nucleus traveling at speeds close to the speed of light compared to the observer. The model is based upon the fundamental principles of QCD and describes the nucleus as a wall of gluonic matter that is very dense, disordered and has semi-fixed particle positions due to Lorentz time dilation. [13]

1.3.4 – Non-flow effects

Several effects, called non-flow, can affect the v_n we measure after a collision by influencing the azimuthal direction of a particle. These effects are caused by other factors than the initial state of the produced matter, making it harder to measure the actual elliptic flow. To overcome this problem, some analysis models try to reduce the effect of non-flow. This is discussed in more detail in the next chapter.

Chapter 2

Flow analysis methods

To analyse the flow for all the particles, of the different particle species, which are created after the heavy-ion collision, multiple analysis methods have been invented to get the most accurate and significant flow values. In section one of this chapter some of these analysis methods are described. How these methods are used is explained in section two. Section three explains how these methods are tested and section four shows the special case of indirect flow measurement in which an initial analysis step is required before being able to measure the flow of specific particles.

2.1 – Event plane, SP, QC

As mentioned in chapter 1.3, we cannot directly measure the reaction plane of an event. Different methods have been developed, in order to find the v_2. These methods can reconstruct the reaction plane, like the event plane method, or work around the lack of a reaction plane by the use of multi particle correlations. All the methods make use of the so called Q-vectors (flow vectors) of the detected particles [4]:

$$Q_n \equiv \sum_{j=1}^{M} e^{in\phi_j} \tag{2.1}$$

Where Q_n is the flow vector for the nth harmonic, M is the multiplicity of the event and ϕ_j is the azimuthal angle of an outgoing track in the laboratory frame.

2.1.1 – Event plane method

The event plane method is one of the most intuitive methods to analyse H.I.C. flow. In this method, the reaction plane angle Ψ_R is estimated for every event by using the Q-vectors of a set of reference particles. These reference particles are all the particles generated by the collision except the particles of which we want to measure the flow. Those particles of which we want to know the flow are called the particles of interest and the estimated reaction plane angle is called the event plane angle Ψ_{EP}. Particles used to estimate the reaction plane cannot be used to measure flow since this would introduce an unwanted correlation between the azimuthal angle of a particle and the event plane angle. Mathematically the anisotropic flow coefficients are described as follows by the event plane method [4, 11]:

$$v_n\{EP\} \equiv \frac{1}{R}\langle\cos\big(n(\phi - \Psi_{EP})\big)\rangle \tag{2.2}$$

With $R = \langle\cos\big(n(\Psi_{EP} - \Psi_R)\big)\rangle$ as the event plane resolution.

2.1.2 – Scalar product method & Q-cumulant method

The scalar product and the Q-cumulant methods use multi particle correlations to reduce systematic non-flow effects. They calculate the flow for a group of particles of interest with the use of the remaining particles as reference particles.

Both these methods were used for the validation of the On-The-Fly model that is described in the next chapter.

2.2 – Analysis models (by aliroot)

The methods used to analyse flow have to be applied to many events. This can be done by writing an analysis macro that can run on the aliroot framework, a C++ framework developed for the ALICE experiment as an extension of the ROOT framework. [4] The analysis macros used in this thesis are AnalyseEventsOnTheFly and TwoParticleResonanceFlowOnTheFly. The generator used for both analysis macros is the macro: GenerateEventsOnTheFly. All files can be found on:

http://svnweb.cern.ch/world/wsvn/AliRoot/trunk/PWGCF/FLOW/macros/GenerateEventsOnTheFly.C
http://svnweb.cern.ch/world/wsvn/AliRoot/trunk/PWG/FLOW/Base/AliFlowOnTheFlyEventGenerator.cxx
http://svnweb.cern.ch/world/wsvn/AliRoot/trunk/PWG/FLOW/Base/AliFlowOnTheFlyEventGenerator.h

2.3 – Quality assessment (QA) of analysis models

In order to know whether an analysis model will return correct results after analysing the data from real heavy ion collisions, its quality needs to be assured. This can be done by using a generator macro that produces a dataset of virtual collisions, that the analysis macro can analyse, and a dataset of the values the analysis model should return. When the analysis macro returns the right values and the generator works properly, it can be concluded that the analysis model is correct.

2.4 – Indirect flow measurement

If a particle decays shortly after the hadronization of the matter formed in a particle collision, then it cannot be observed directly. If it was a single decay, in which the decay products are known, the existence and properties of the decayed particle could be deduced by looking at the energy and momenta of the decay products. We no longer know, however, which particle belongs to which decay, for particles that end their short existence directly after a heavy ion collision, because of the background noise of other particles. Therefore we will need to use more complicated and time intensive methods to find their v_2 values.

Assuming a particle decays into two particles, that do not decay themselves, we can use a statistical reconstruction of the flow of the particle by looking at the invariant mass spectrum of all pair combinations of the particles that are the same as the decay products. The invariant mass spectrum of all pair combinations can be seen as a correlated part, a peak in the spectrum due to the correlated decay products of the

decayed particle, and an uncorrelated part of all combinations of the background particles with other background particles or decay product particles [4]:

$$N^{Pairs}(m_{inv}) = N^{bg}(m_{inv}) + N^{DP}(m_{inv}) \tag{2.3}$$

We can use this to find the flow of the decayed particles by rewriting the next equation:

$$N^{Pairs}(m_{inv})\, v_n^{Pairs}(m_{inv}) = N^{bg}(m_{inv})\, v_n^{bg}(m_{inv}) + N^{DP}(m_{inv})\, v_n^{DP}(m_{inv}) \tag{2.4}$$

Into:

$$v_n^{DP}(m_{inv}) = \frac{N^{Pairs}(m_{inv})}{N^{DP}(m_{inv})} v_n^{Pairs}(m_{inv}) - \frac{N^{bg}(m_{inv})}{N^{DP}(m_{inv})}\, v_n^{bg}(m_{inv}) \tag{2.5}$$

A detailed description of how this formula should be used to get the elliptic flow for a type of particle is given in [4].

Chapter 3

Flow analysis on the fly

In order to improve the elliptic flow measurement in heavy ion collisions, a new simulation model, called "on the fly", has been developed. This simulation model is made to help test (new) flow analysis methods as is explained in section 1 of this chapter. How the heavy-ion collisions are simulated in the new model is explained in section 2. In section 3 we will explain the data we used for the quality assessment of the new model and in section 4 we will discuss the most important results of this QA.

3.1 – Improved Analysis

Some of the particles produced in H.I.C. can be detected directly by a detector, along with their properties like momentum and electric charge, while others decay into different particles that might be detected or decay into other particles as well and so on. Because of the different properties of the particles, we can identify different particle species. These species, or their parton components, might have interacted differently during their formation than other particles. This different interaction can result in a species dependent anisotropic flow.

The on-the-fly model is made to mimic this species specific v_2 property. Because of this, we will be able to use the new model as the QA basis for (new) flow analysis methods.

3.2 – Basics of the on-the-Fly model

The On-The-Fly simulation is done by running the GenerateOnTheFly macro on the aliroot framework. In the code you enter several fields to determine what kind of events you will simulate. You declare which particle species you want to create, how many particles you want to create for each particle type, how large the background needs to be, whether particle species get a specific v_2 value, how many events you want to create and if particle should be allowed to decay or not. After all the information has been provided, the model will start simulating the events one at a time. The particle tracks created in an event are distributed randomly in ϕ, Ψ_R and η. The particles are then given an azimuthal distribution by an afterburner. The afterburner creates a new azimuthal distribution by changing the azimuthal angles off all tracks by a factor that is dependent on the azimuthal angle of the particle track and the specified v2 value for the type of particle belonging to that track [14]:

$$\phi = \phi_0 - \tilde{v}_2 \sin[2(\phi - \Psi_R)] \tag{3.1}$$

With ϕ being the final azimuthal angle of the particle, ϕ_0 the original azimuthal angle of the particle and $\tilde{v}_2 \approx v_2(p_t)$. Particles can then be decayed by using the Pythia decayer. The simulated events are stored on the computer for further use.

3.3 – QA data

For the quality assessment of the 'on the fly' simulation model we have made several sets of histograms for all generated particle species. These sets have four basic histograms and three combined histograms as can be seen in the figures 3.1 and 3.2. In this section we describe all these histograms.

Reaction plane angle histogram - The calculated reaction plane angle for each event is saved in this histogram. Its values should lie between $-\pi$ and π. We make this histogram to check if the generated values lie within this range.

Transverse momentum spectrum histogram – In this histogram the number of particles that have a specific p_t value are shown as a function of p_t. The resulting distribution is fitted to the graph of the generated p_t distribution. We want to check if the results match the generated distribution and if it changes when decay products are added for specific particle species.

Eta histogram - The amount of particles measured on the longitudinal (in contrast to radial) side (η) of the detector. Particles are generated to fit between -1 and 1. We make this histogram to check if the generated values lie within this range.

Azimuthal angle histogram - The azimuthal angle from the laboratory coordinate system to the particle (see fig. 1.4) is saved in this histogram.

Azimuthal angle of particle minus Reaction plane angle histogram - The calculated azimuthal particle distribution is saved in this histogram. If there is no anisotropic flow then the distribution should be flat. If there is an elliptic flow the distribution should be sinusoidal.

Transverse momentum versus Azimuthal particle distribution histogram - The Transverse momentum and the Azimuthal particle distribution are plotted against each other in this 3D plot.

Elliptic flow as a function of transverse momentum histogram - The calculated v_2 for every particle is saved and added to its corresponding p_t value in this histogram. At the same time the graph of the generated v_2 value for this particle species is plotted in the histogram. The calculated v_2 should match the graph of the generated v_2 value. If there are decay contributions to the particle species of this histogram than we expect a modified v_2 spectrum.

3.4 – QA results of the on-the-fly model

A selection of the QA histograms has been added in the appendix. We will refer to these figures while we discuss the QA of the on-the-fly model.

Figure 1 and 2 are the analysis output for a dataset of 5000 events with no decay and the Phi-meson as the particle of interest. In these figures the analysis shows us that the on-the-fly model generates realistic values for Ψ_R, ϕ, η and the analysis returns a v_2 value that match the generated v_2 function very well. Also, the azimuthal angle distribution shows the expected sinusoidal property.

Figure 3 till 6 display the analysis output for a dataset of 5000 events with no decay and the Kaon$^+$ and Kaon$^-$ mesons as the particles of interest. In these figures we check the difference in the analysis output when adding v_2 or no v_2 to the generated particles. The data in figure 3 and 4 are the analysis output of the dataset with v_2 and the data in figure 5 and 6 are the analysis output of the dataset without v_2. In the azimuthal particle distribution graphs of figure 4 and 6 we can see, as expected, that the lack of v_2 changes the azimuthal particle distribution from a sinusoidal to a flat distribution.

In order to check the decay of the Phi meson to the Kaon$^+$ and Kaon$^-$ mesons we look at the analysis output of the Kaon$^+$ and Kaon$^-$ before and after the decay. We used a dataset of 500 events with a large amount of Phi-mesons versus Kaon mesons. In figure 7 and 8 we present the results without decay and in figure 13 and 14 the results with decay. In these results there are three significant differences:

1. The measured p_t distribution is different than the generated p_t distribution. Since this distribution is species dependent, the Kaon mesons that are the result of decay should inherit the characteristics of their parent particles and change the measured p_t distribution.
2. The η distribution no longer fits between -1 and 1. The Phi mesons are generated within a range of $-1 < \eta < 1$, the angles of the Kaons produced by the decay of the Phi meson are, however, not limited to this range. Therefore we should find these particles outside the range of $-1 < \eta < 1$.
3. The number of entries, amount of particles, has changed. This is the result of the extra kaon mesons that have been produced by the decay of other particles.

The generator macro, used for the on-the-fly model, saves whether a particle is an initial particle or a secondary (decay) particle. For the decay QA above, the analysis macro was also used to show the independent analysis results for the initial and secondary Kaons. The initial Kaon results can be seen in figure 9 and 10 and the secondary Kaon result are found in figure 11 and 12. As can be expected, the results of figure 7 and 8 look practically the same as the results of figure 9 and 10.

An unresolved problem that still persist in the GenerateEventsOnTheFly macro is that the macro generates one particle for every declared particle species per event too many. This has had no significant effect on the QA of the on-the-fly model.

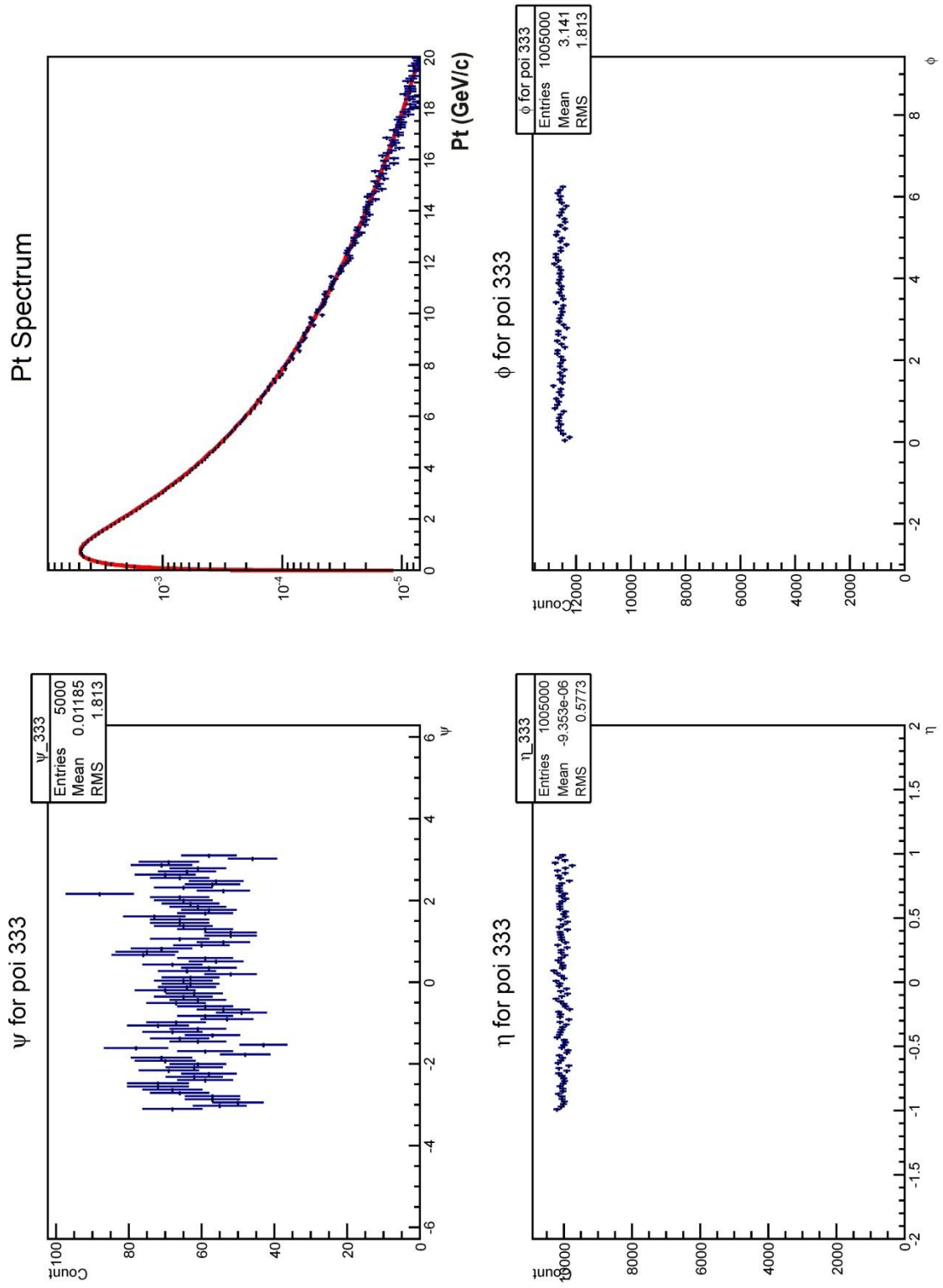

Figure 3.1: QA histograms with Phi-meson results for 5000 events with 200 Phi-mesons per event. No decay.

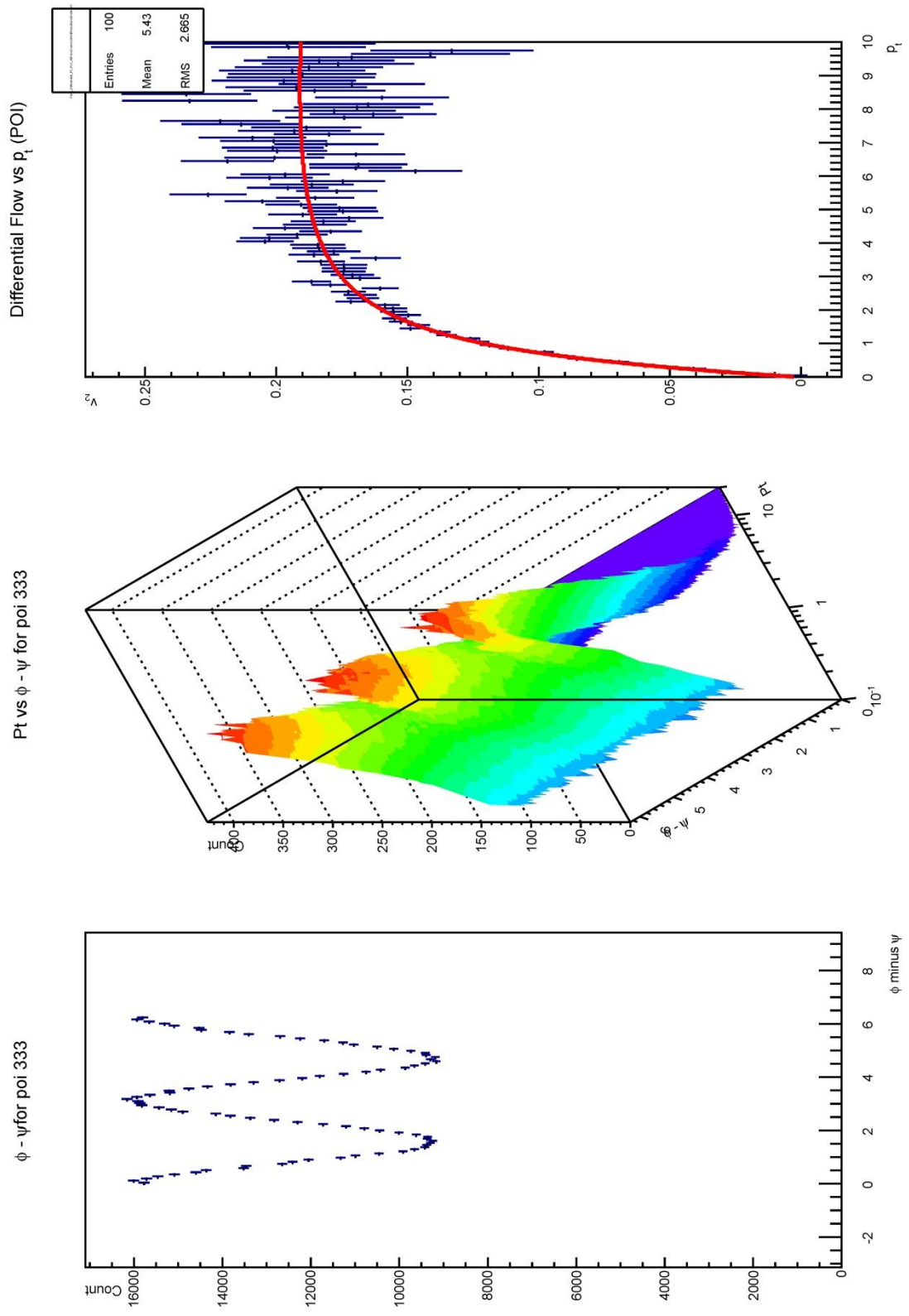

Figure 3.2: QA histograms with Phi-meson results for 5000 events with 200 Phi-mesons per event. No decay.

Chapter 4

Indirect Phi-meson flow measurement

The Phi-meson is expected to have a small hadronic cross section, making it sensitive to collective motion during the partonic phase of the collision and unlikely to undergo scattering during the hadronization of the partonic phase. [4] This makes the Phi-meson a particle of interest since the formation of a QGP results in collective motion of the partons during the partonic phase. Measuring a Phi-meson v_2 would therefore be a strong indication of the formation of a QGP.

We can use the invariant mass method to reconstruct the flow of the Phi-mesons. How this is done is explained in detail in [4]. This method assumes however that all Kaons measured are actual Kaons. The detector used to identify particles after an event has a chance to mistake another particle for a Kaon. In the next sections we will discuss the results of two quality assessments on the effects of these misidentifications on the reconstructed v_2.

4.1 Phi-meson flow reconstruction

In order to reconstruct the Phi-meson flow by using the invariant mass method, we need to know the invariant mass of the Phi-meson and the width of the invariant mass peak in the mass spectrum. These values can be reconstructed using the invariant mass spectrum of the unsigned Kaon pairs as explained in chapter 2.4. An example of the calculated invariant mass spectrum for the Phi-meson is given in figure 4.1.

4.2 QA of Phi-meson flow reconstruction

We check the differences in the analysis results of Phi-meson flow for an uncontaminated analysis, with no misidentification of particles, and for a contaminated analysis, with misidentification of particles. For the contaminated analysis we choose Pions[2] to be misidentified as Kaons with a 50% chance of misidentification. As basis for the analysis we use two sets of simulated events in which we make the generated v_2, for one type of particle, clearly distinguishable from the elliptic flow of the other particle species. In the first set (N_{events}=100.000) we do this for the v_2 of Pions and in the second set (N_{events}=50.000) we do this for the v_2 of Phi-mesons. The amount of particles generated in set 1 is almost four times as high as the amount of particles generated in set 2.

The analysis results for the estimated invariant mass of the Phi-meson are given in figure 4.2 and the estimated mass width is given in figure 4.3. In these graphs it can be seen that the contaminated and uncontaminated analyses give comparable results. The biggest differences are in the low and high p_t ranges, where we also have the lowest amounts of useable data. Between the sets there seems to be a

[2] In our simulations the ± Pions are generated the most abundant of all the particles so that if they effect the Phi-flow reconstruction by being misidentified it will result in a clear deviation.

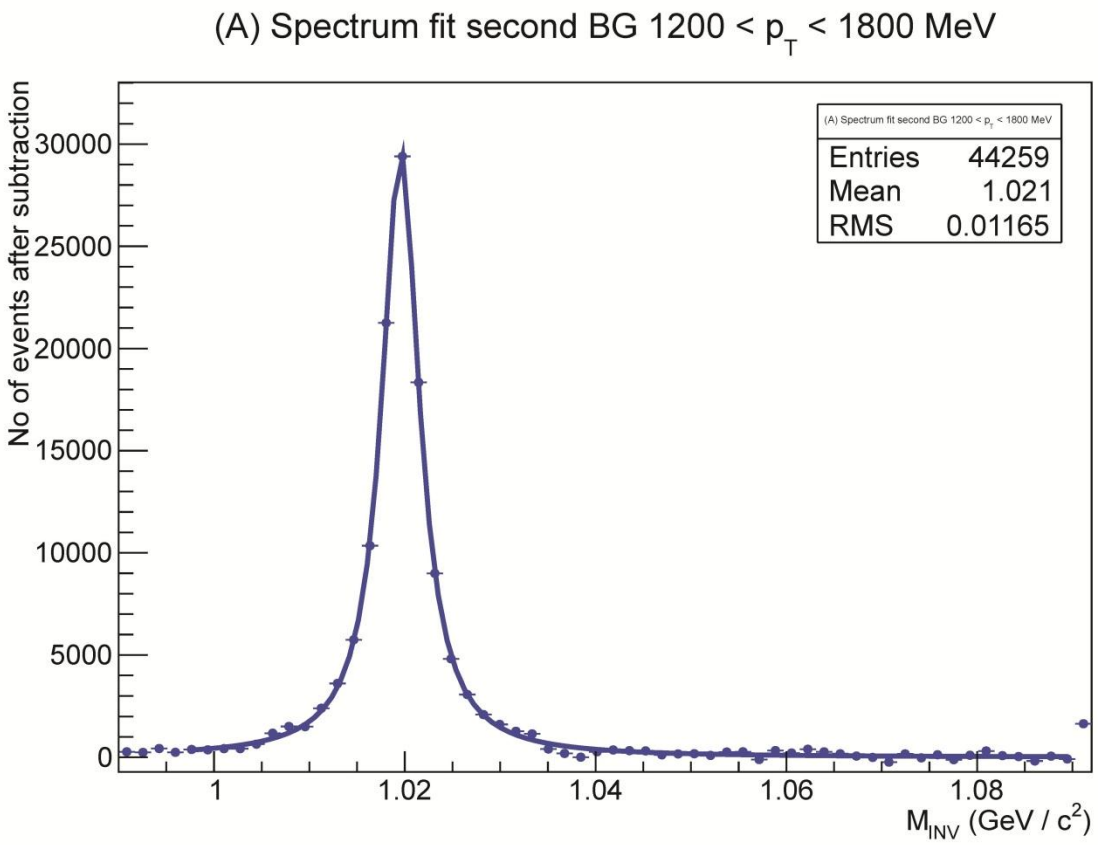

Figure 4.1: The reconstructed invariant mass peak for the Phi-meson, based upon particles measured within 1.2 GeV < p_t < 1.8 GeV.

bigger difference in the results of set 2 than in the results of set 1. Since there are a lot more particles used in set 1 than in set 2, it is reasonable to contribute this difference to the higher statistical significance of set 1.

The elliptic flow of the Phi-meson is measured, using the estimated values for the mass and mass width of the Phi-meson. The results are plotted in figure 4.4, for set 1, and in figure 4.5, for set 2. The reconstruction method fails above approximately $p_t = 2.4\ GeV$ because there is not enough data. Therefore, only the first four points, in each graph, should be used.

The v_2 reconstruction results appear to be too uncertain to give an accurate answer on the question whether misidentification of Pions will lead to a wrong measurement of the Phi-meson flow.

In figure 4.6 and 4.7 the raw Phi-meson and background yields are presented. A contaminated dataset appears to result in a slightly higher Phi-meson yield and an expected higher (Kaon) background yield.

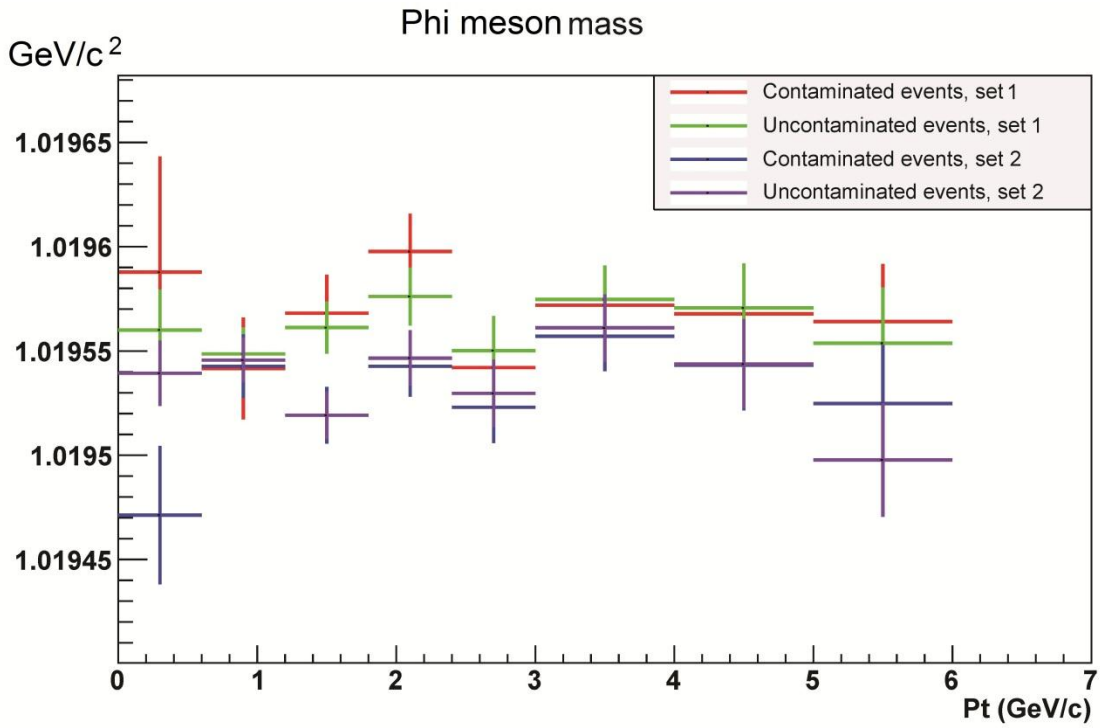

Figure 4.2: The estimated Phi-meson mass, calculated using Kaons within a specific transverse momentum range. - Set 1: Red shows the contaminated and green the uncontaminated analysis. - Set 2: Blue shows the contaminated and purple the uncontaminated analysis.

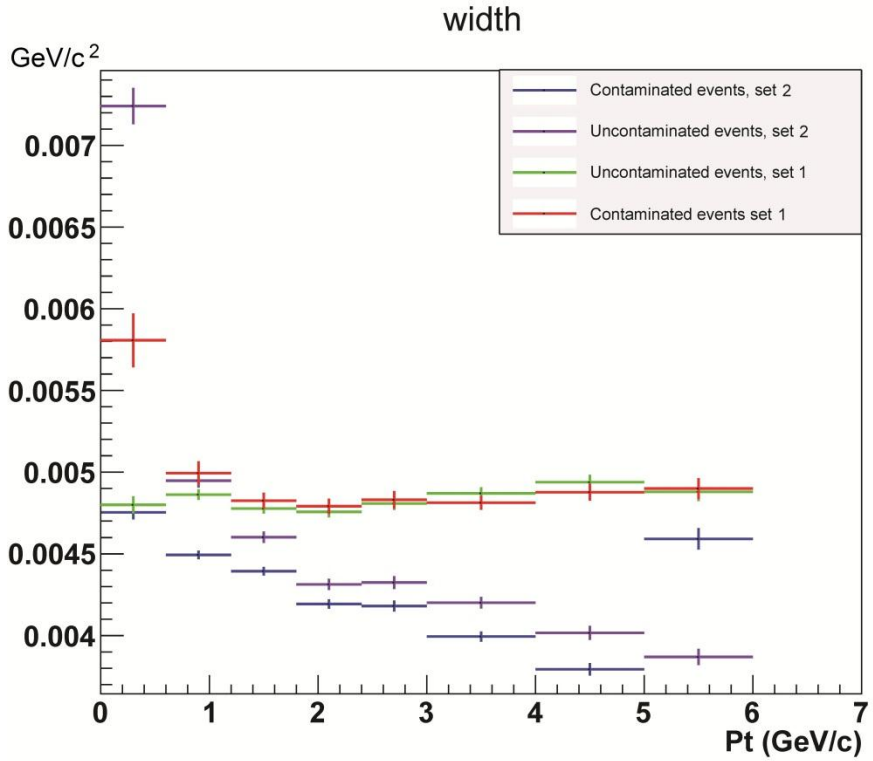

Figure 4.3: The estimated Phi-meson mass width, calculated using Kaons within a specific transverse momentum range. - Set 1: Red shows the contaminated and green the uncontaminated analysis. - Set 2: Blue shows the contaminated and purple the uncontaminated analysis.

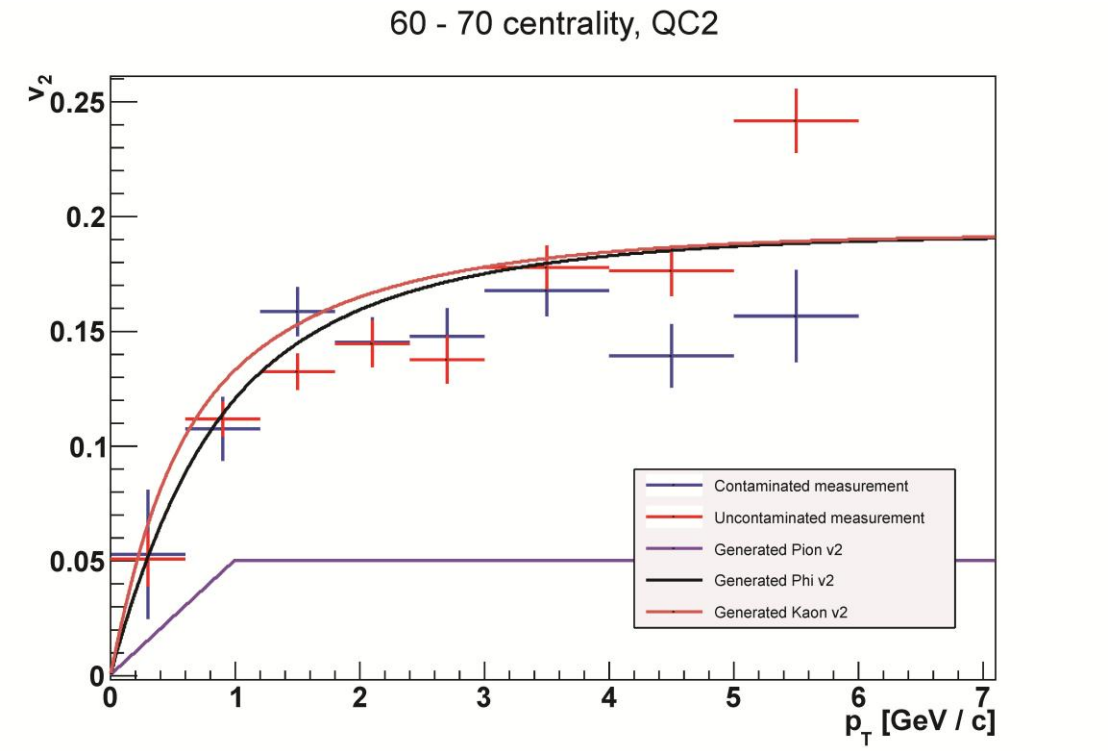

Figure 4.4: - Set 1: The graph shows the generated v_2 for several particles (brown: Kaon, black: Phi-meson and purple: Pion) and the estimated Phi-meson v_2 for a contaminated (blue) and an uncontaminated (red) analysis.

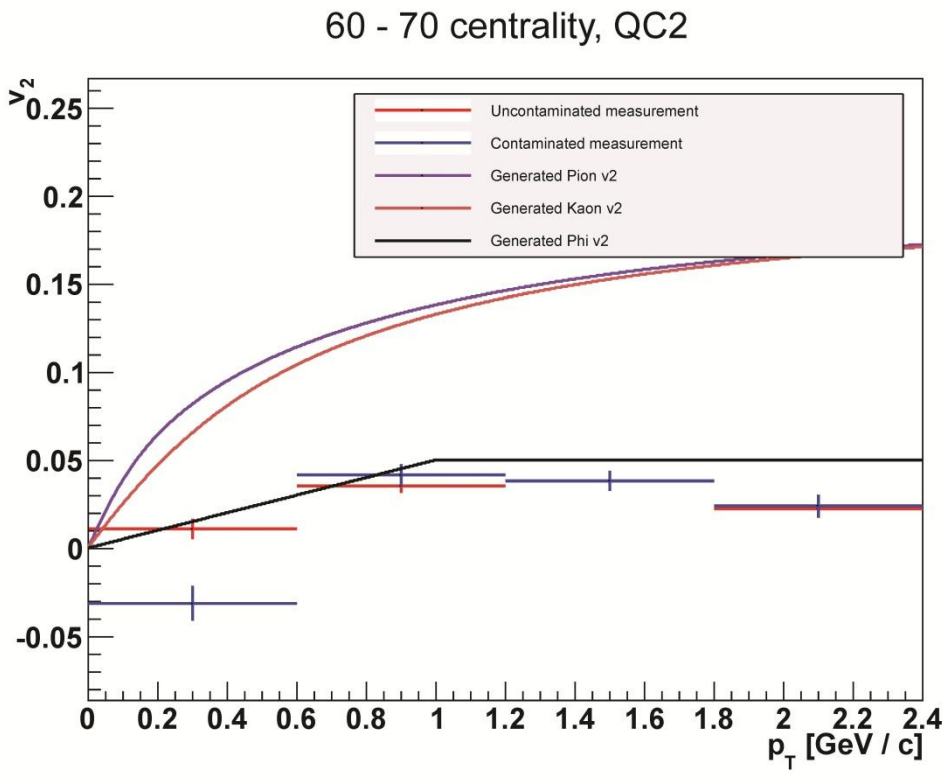

Figure 4.5: - Set 2: The graph shows the generated v_2 for several particles (brown: Kaon, black: Phi-meson and purple: Pion) and the estimated Phi-meson v_2 for a contaminated (blue) and an uncontaminated (red) analysis.

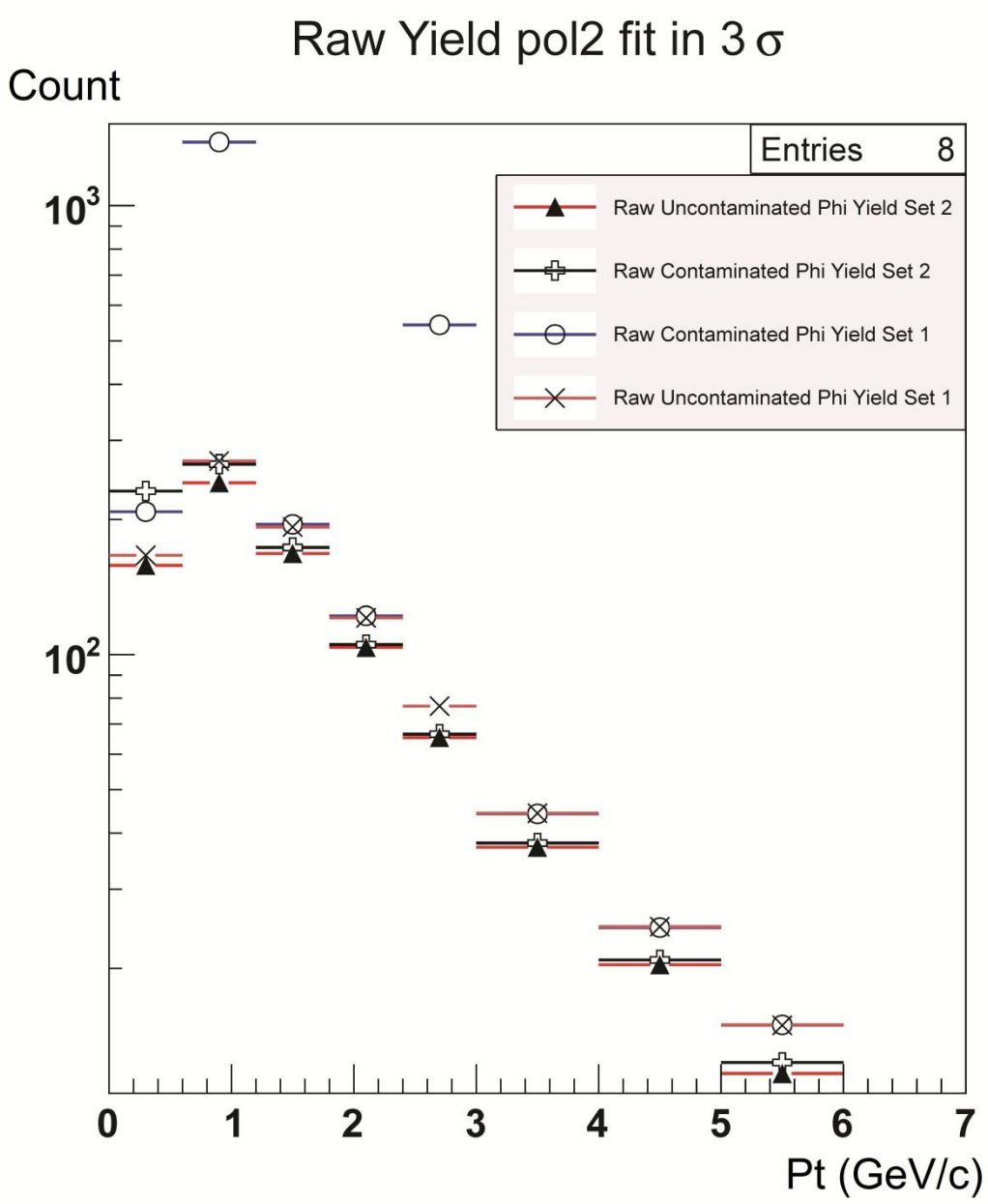

Figure 4.6: A graph of the number of reconstructed Phi-mesons as a function of p_t.

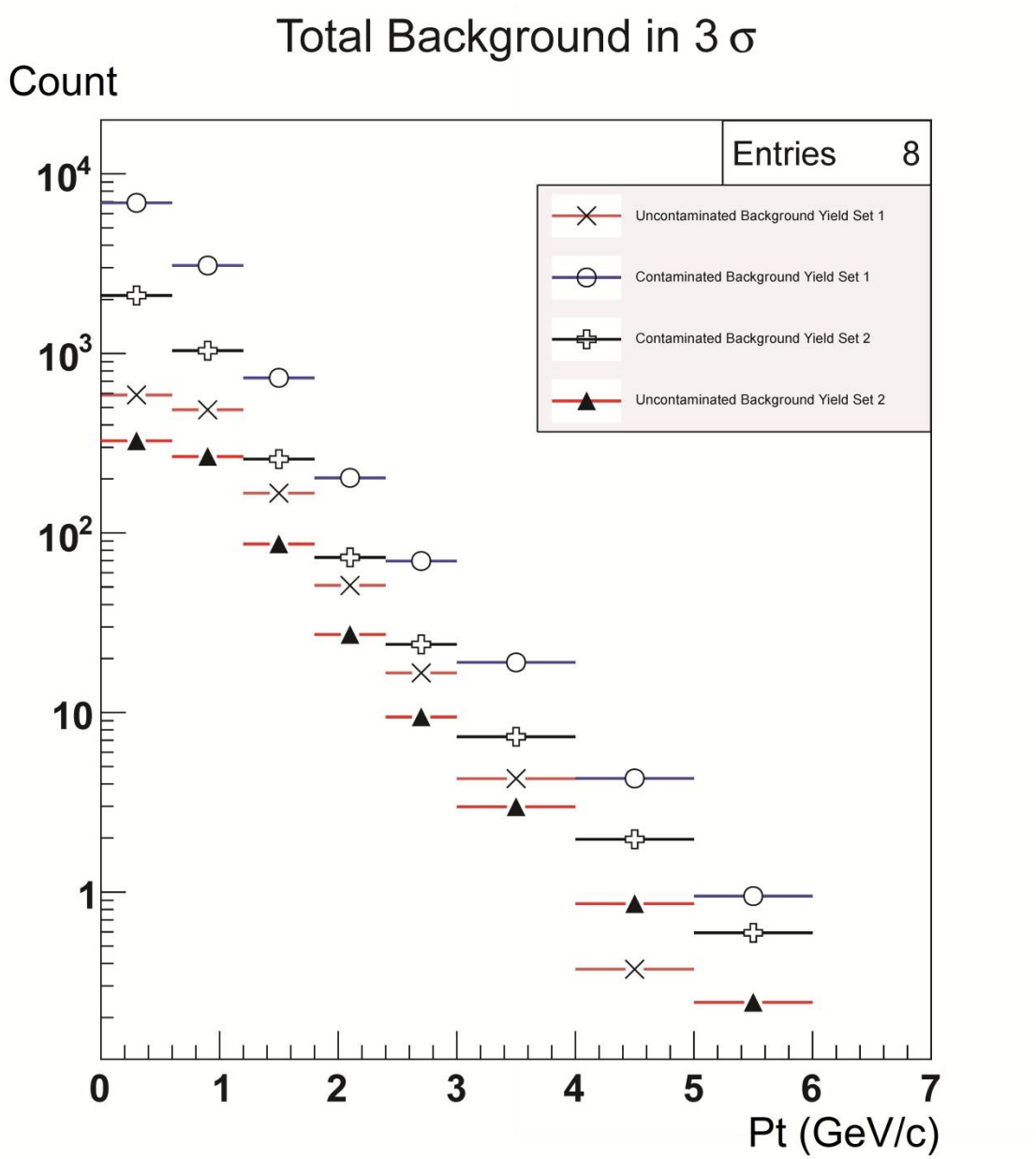

Figure 4.7: A graph of the number of plus or minus Kaons as a function of p_t.

Chapter 5

Conclusion, discussion and outlook

The quality assessment of the on-the-fly simulation model has shown that the model is capable of generating heavy-ion collision simulations that fit the expected parameters. The model correctly decays particles and changes the v_2 values for those particle species.

In the Phi-meson flow reconstruction, the differences between the contaminated and uncontaminated analyses in reconstructing the Phi-meson mass and mass width seem small for most data points. The statistical significance is however too low to conclusively determine if there is a statistical difference in calculated mass, mass with and elliptic flow values for a contaminated dataset versus an uncontaminated dataset.

A problem with the method of flow reconstruction for decayed Phi-mesons is its high CPU requirement. This CPU requirement rises rapidly for more central collisions, because combinations are made for all Kaons in an event. When only peripheral collisions are used, this method requires data of a large number of events before it gives statistical significant results.

Next research goals are redoing the QA of the flow reconstruction with a larger number of events and/or particles, to increase the speed of the flow reconstruction and to use the On-The-Fly model to look at higher flow harmonics.

Bibliography

[1] A. Bilandžić, PhD thesis, "Anisotropic Flow Measurements in ALICE at the Large Hadron Collider", Utrecht University, 2012.

[2] Y. Bai, PhD thesis, "Anisotropic Flow Measurements in STAR at the Relativistic Heavy Ion Collider", Utrecht University, 2007.

[3] E.L. Simili, PhD thesis, "Eliptic Flow Measurements at ALICE", Utrecht University, 2008.

[4] R.A. Bertens, MSc thesis, "Azimuthal anisotropy of φ-mesons in $(S_{NN})^{1/2}$ = 2.76 TeV Pb-Pb Collisions at ALICE", Utrecht University, 2012.

[5] Donald H. Perkins: Introduction to High Energy Physics, fourth edition, (Cambridge University Press, Cambridge, 2000).

[6] A. Das and T. Ferbel: Introduction to Nuclear and Particle Physics, second edition, (World Scientific, Singapore, 2003).

[7] F.Karsch and E.Laermann: arXiv:hep-lat/0305025

[8] W.A. Zajc: arXiv:0802.3552

[9] T.Hirano, N. van der Kolk, A.Bilandzic: arXiv:0808.2684

[10] R. Snellings: arXiv:1102.3010

[11] A. Bilandzic, N. van der Kolk, J. Ollitrault, R. Snellings: arXiv:0801.3915

[12] A. Bilandzic, R. Snellings, S. Voloshin: arXiv:1010.0233

[13] L. McLerran: arXiv:hep-ph/0104285

[14] M. Masera, G. Ortona, M. G. Poghosyan, and F.Prino: 210.1103/PhysRevC.79.064909

List of used abbreviations and symbols

b	Impact parameter
CGC	Colour Glass Condensate
E	Energy
EoS	Equation of State
η	Pseudo rapidity
fm	Femtometer
H.I.C.	Heavy-Ion Collision
MeV	Mega electron-volt
GeV	Giga electron-volt
p	Momentum
p_t	Transverse momentum
ϕ	Azimuthal particle angle
Ψ_{EP}	Event plane
Ψ_R	Reaction plane
QA	Quality Assessment
QC	Q-Cumulant method
QCD	Quantum Chromo Dynamics
QED	Quantum Electrodynamics
QGP	Quark-Gluon Plasma
R	Event plane resolution
SP	Scalar product method
v_n	Flow coefficient
v_2	Elliptic flow
y	Rapidity

Acknowledgements

First of all I would like to thank Raimond Snellings for the opportunity to do my thesis at his group and his willingness to answer all my questions when I took his bachelor-course in subatomic physics. Most of all I would like to thank Redmer Bertens for all his help, support and supervision during the last few months. His clarity when explaining something, his fast reactions on e-mails and his unwavering willingness to help solve coding problems have made most of this thesis possible. I would like to thank You Zhou and Carlos Lara for helping me start with all I had to do for this thesis. I also would like to thank Andrea Dubla for his help. And last but not least I would like to thank Marco van Leeuwen for coordinating the bachelor thesis program, helping with computer problems and always being able to solve the coding problems when no one else seemed able to do so.

Appendix

The graphs on the next pages show the results described in chapter 3.4. The particle codes of the Particle Data Group convention were used. These codes represent different particles. The codes that are used in the following graphs are:

321 → ± Kaon

333 → Phi-Meson

Appendix Figure 1

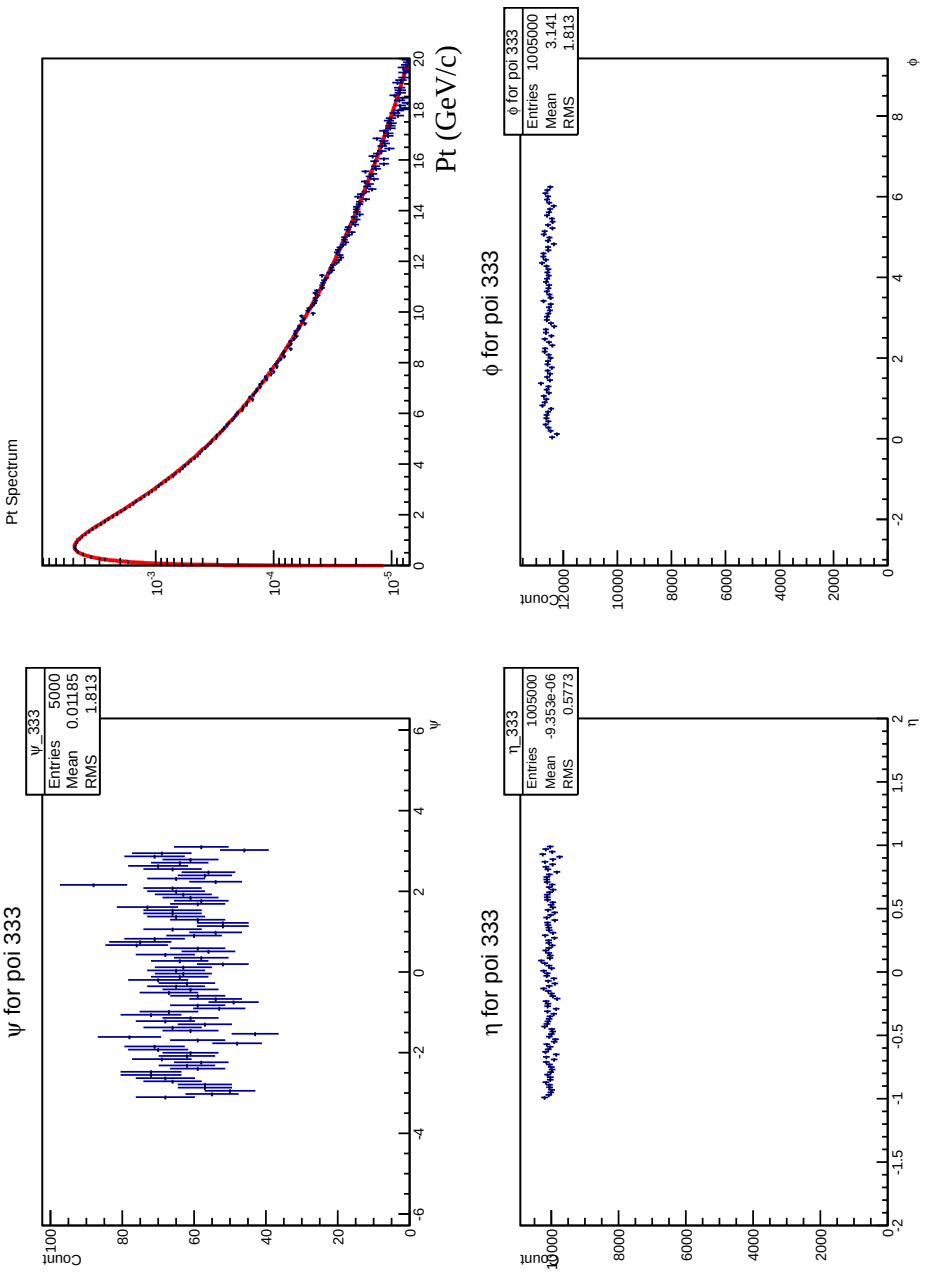

Appendix Figure 2

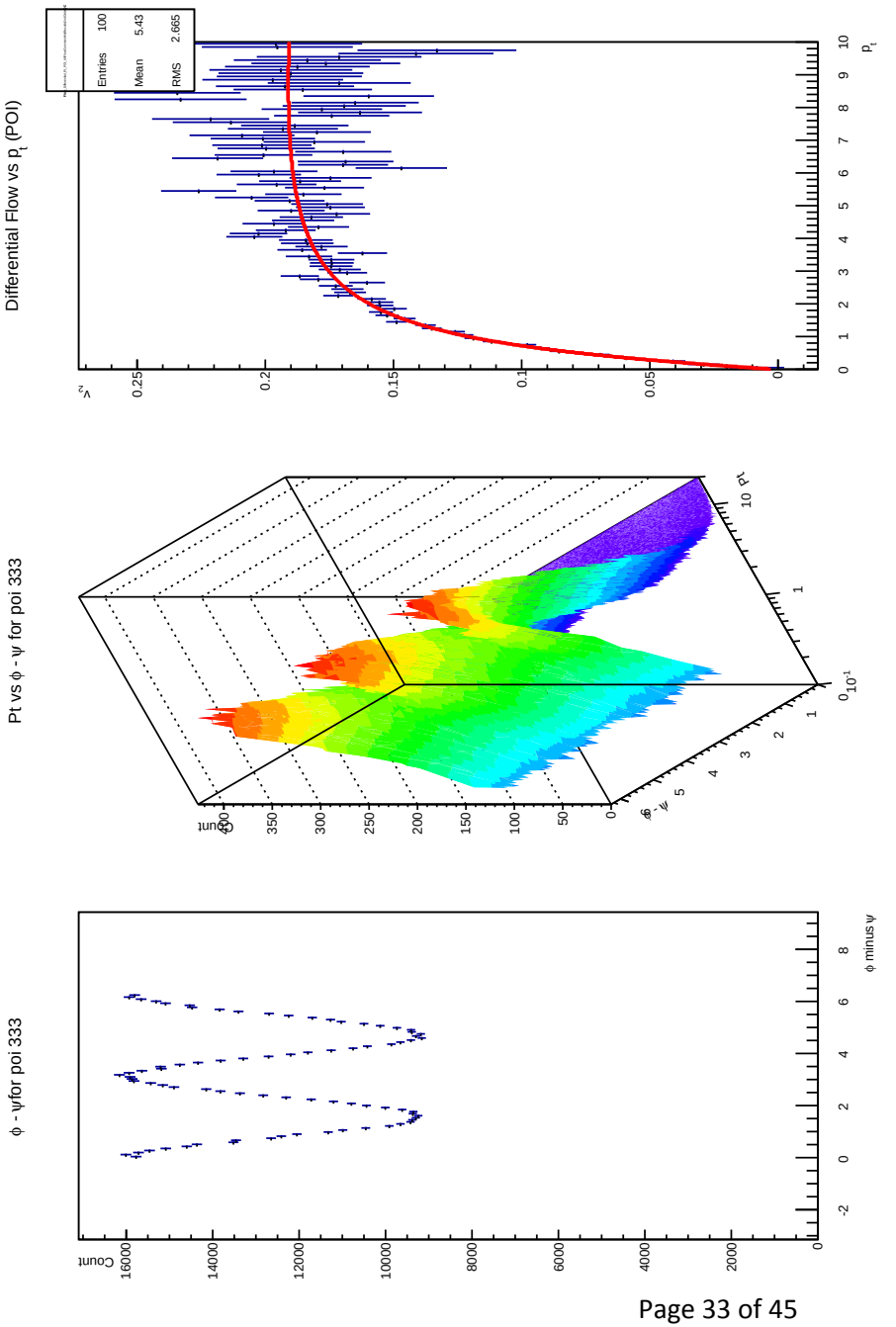

Appendix Figure 3

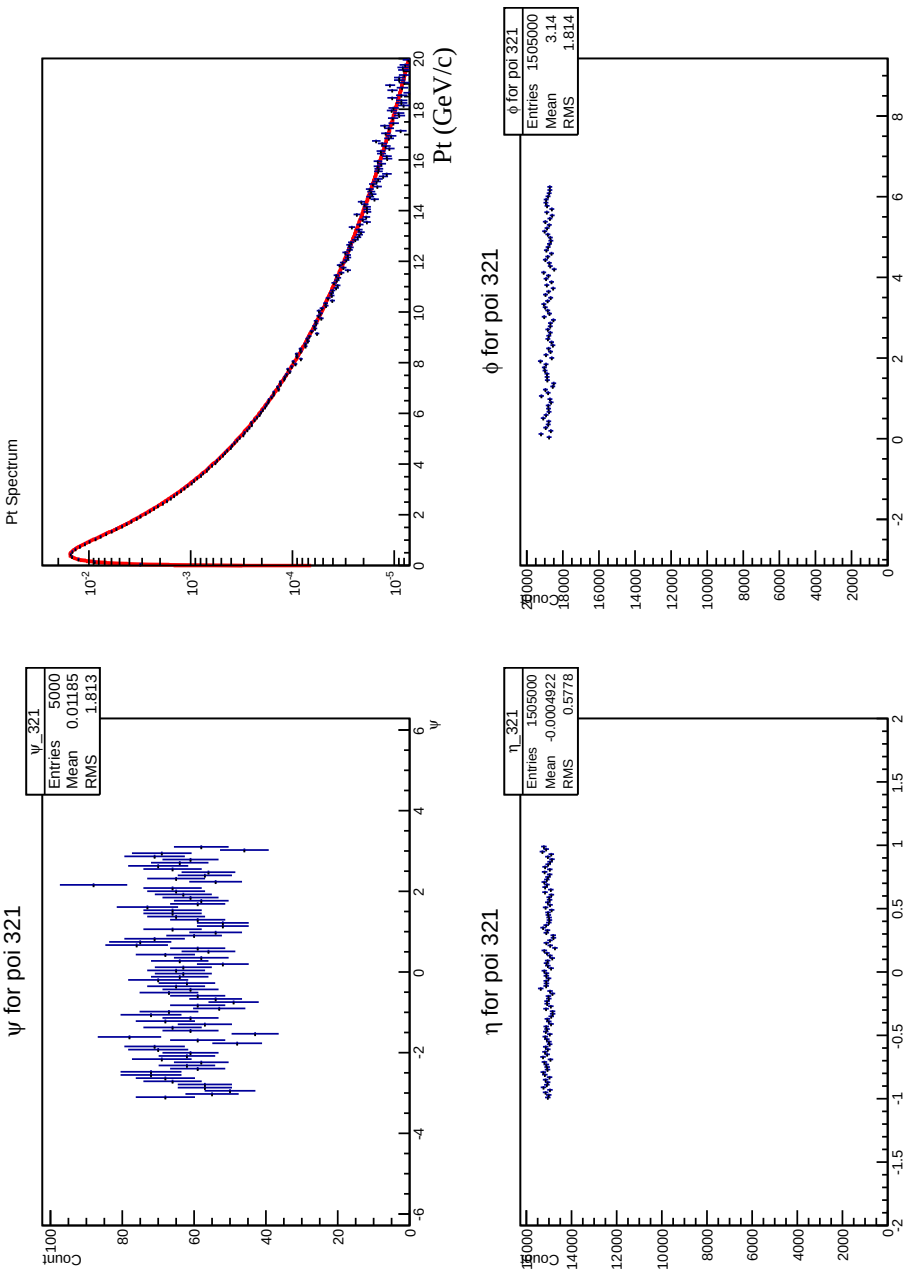

Appendix Figure 4

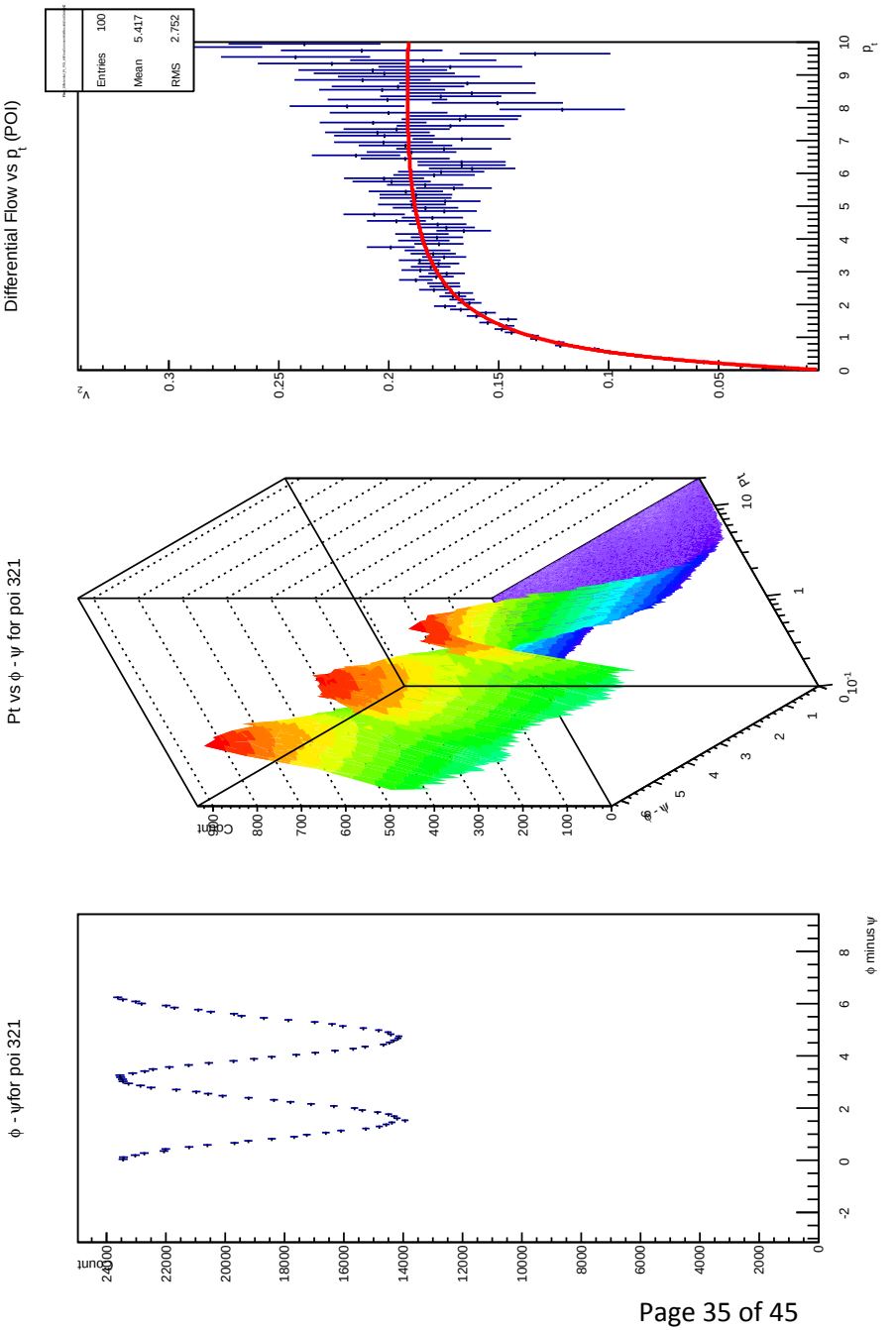

Appendix Figure 5

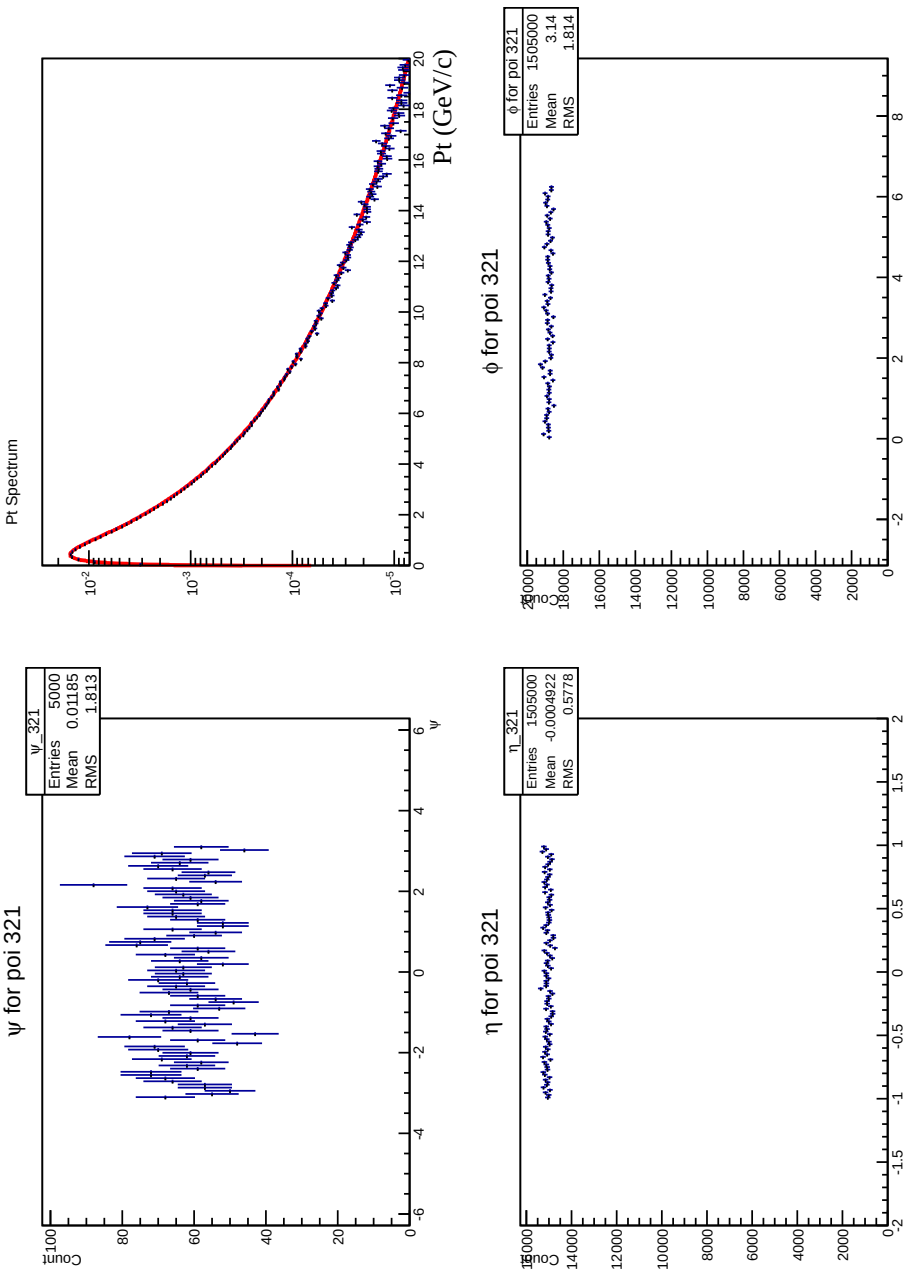

Appendix Figure 6

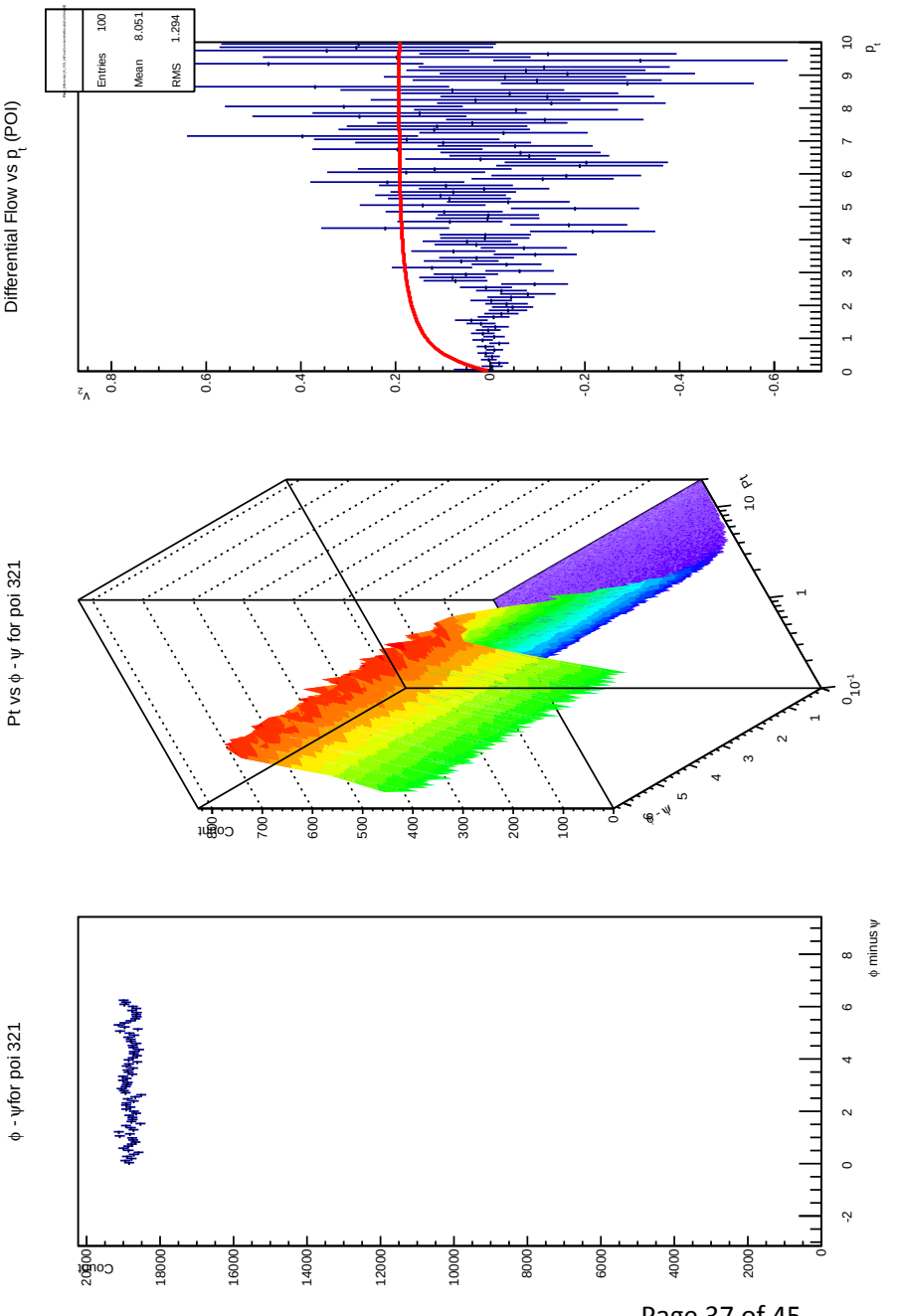

Appendix Figure 7

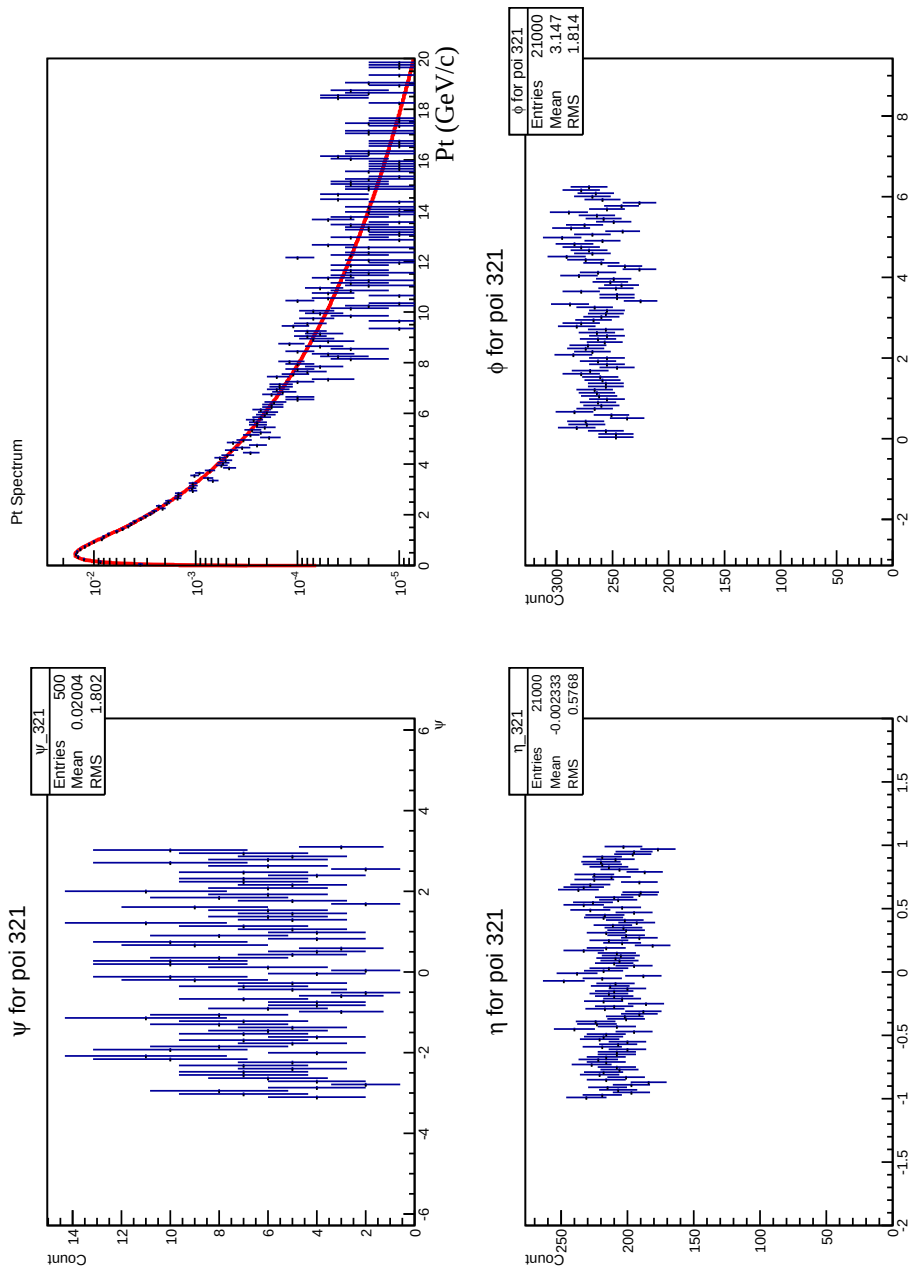

Appendix Figure 8

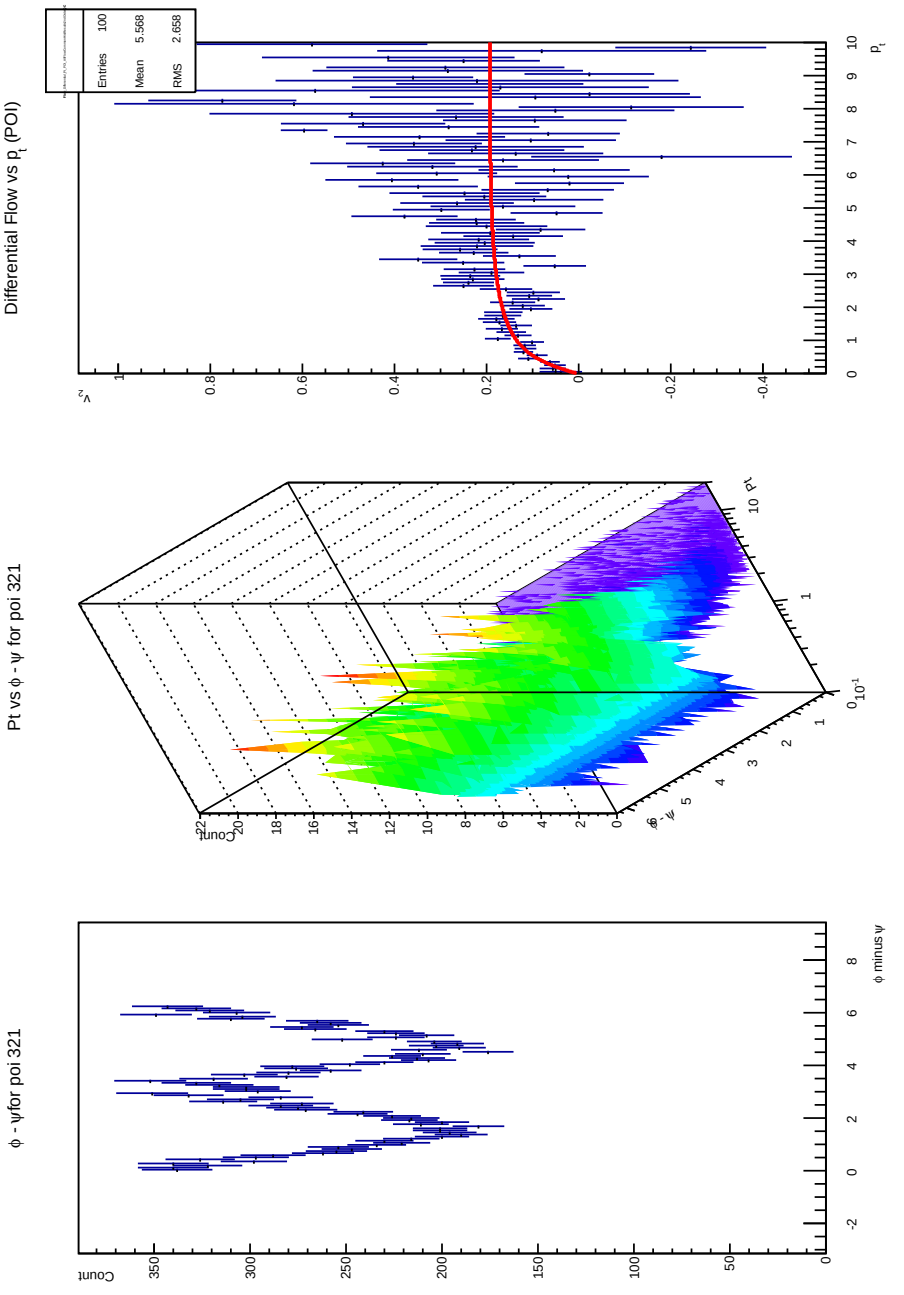

Appendix Figure 9

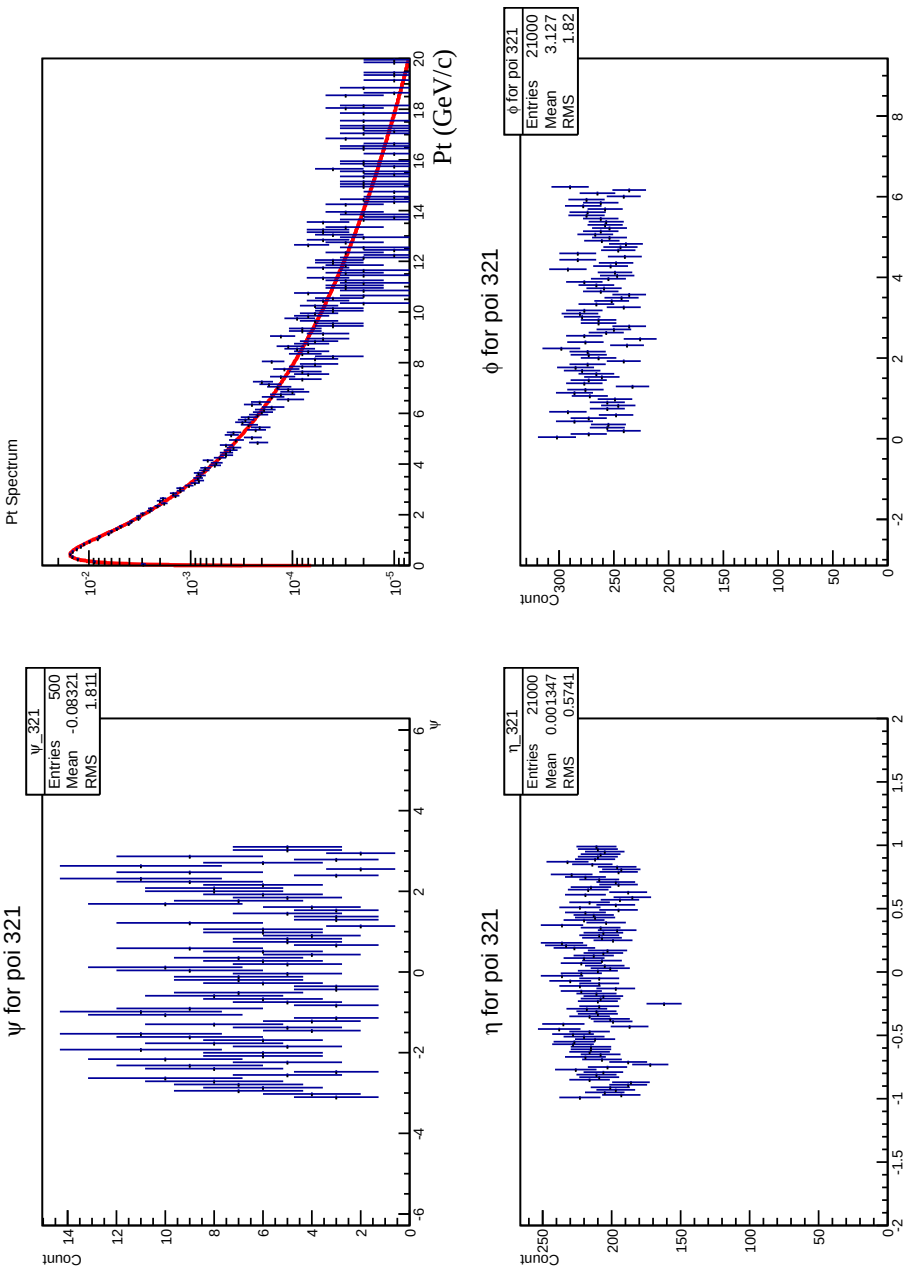

Appendix Figure 10

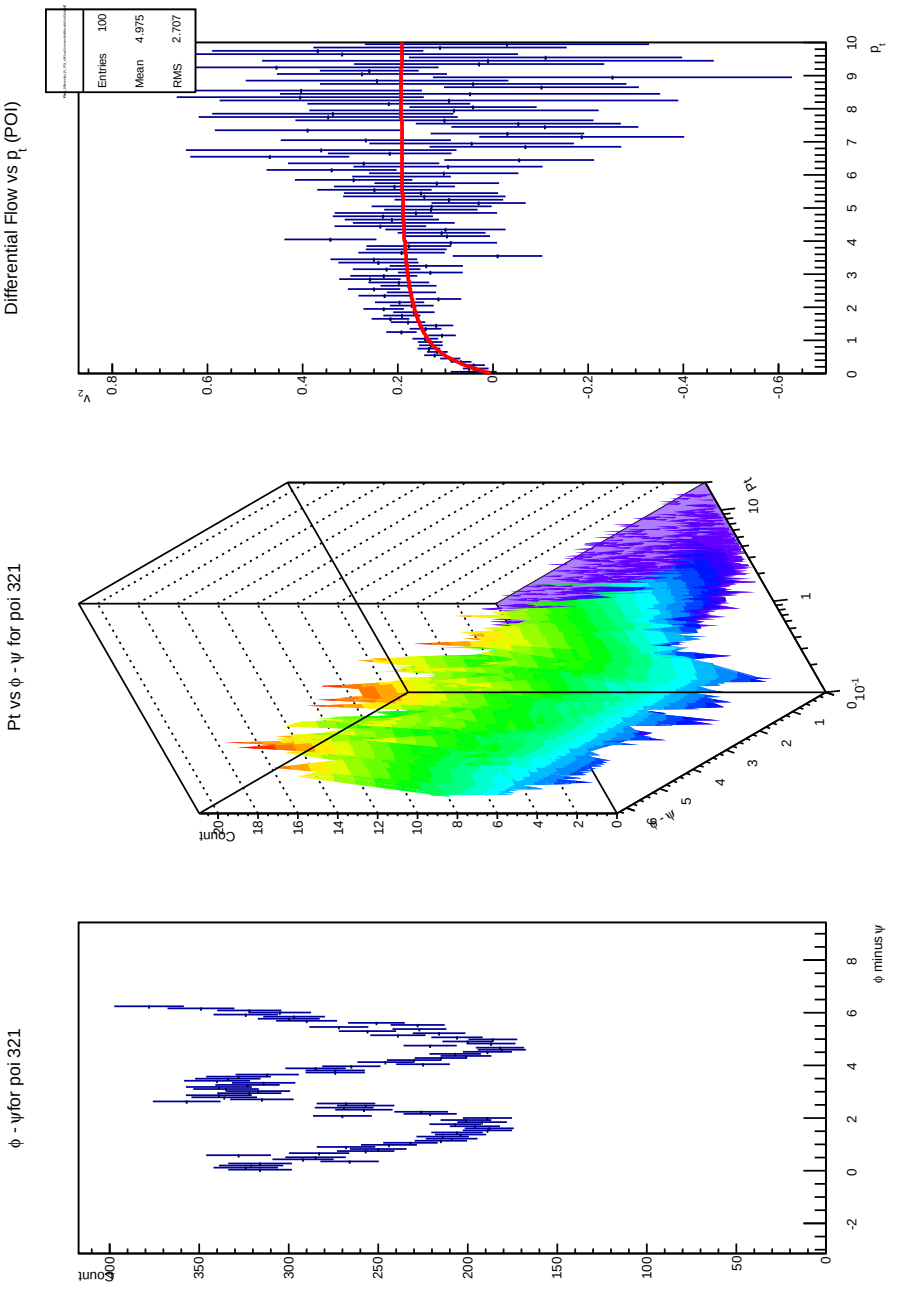

Appendix Figure 11

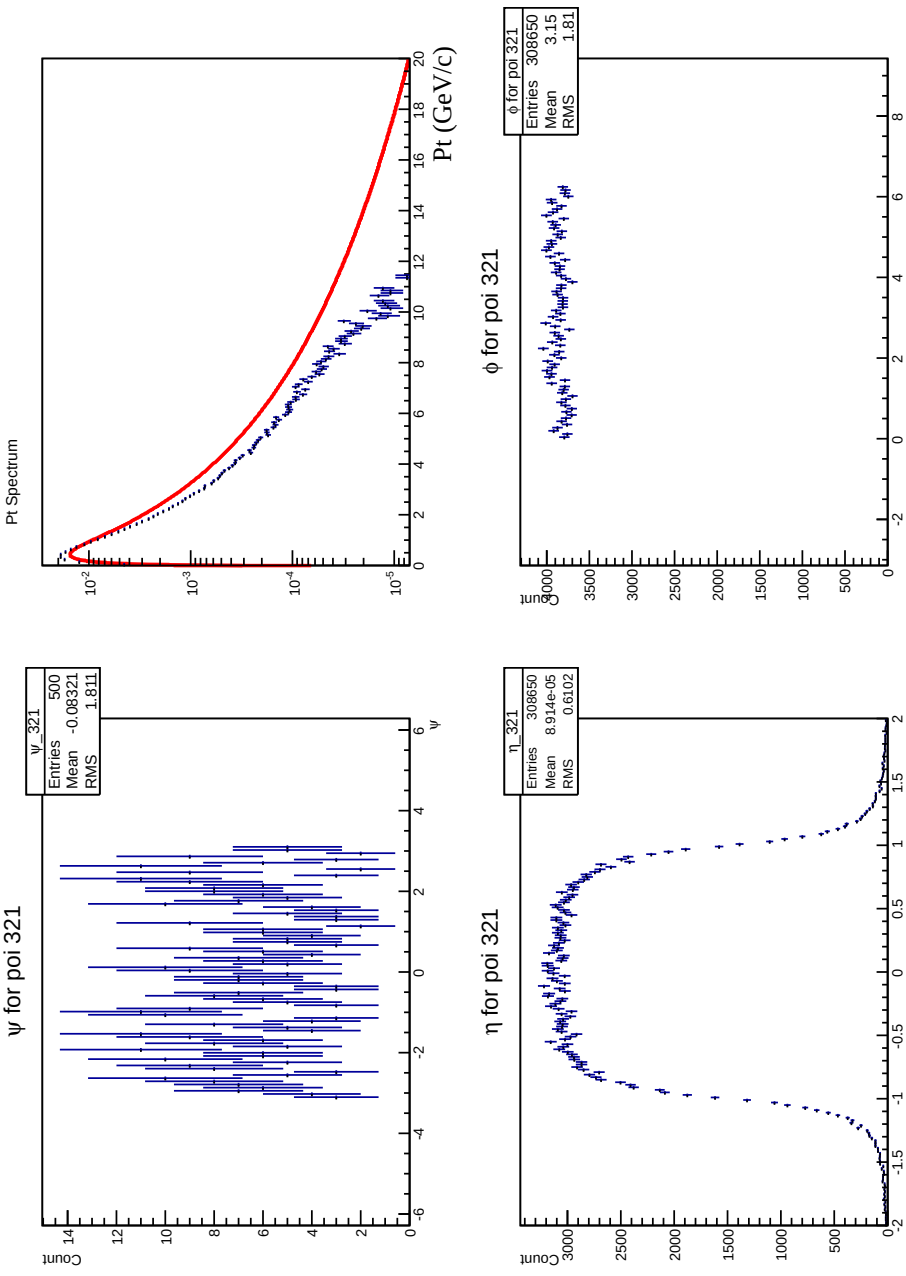

Appendix Figure 12

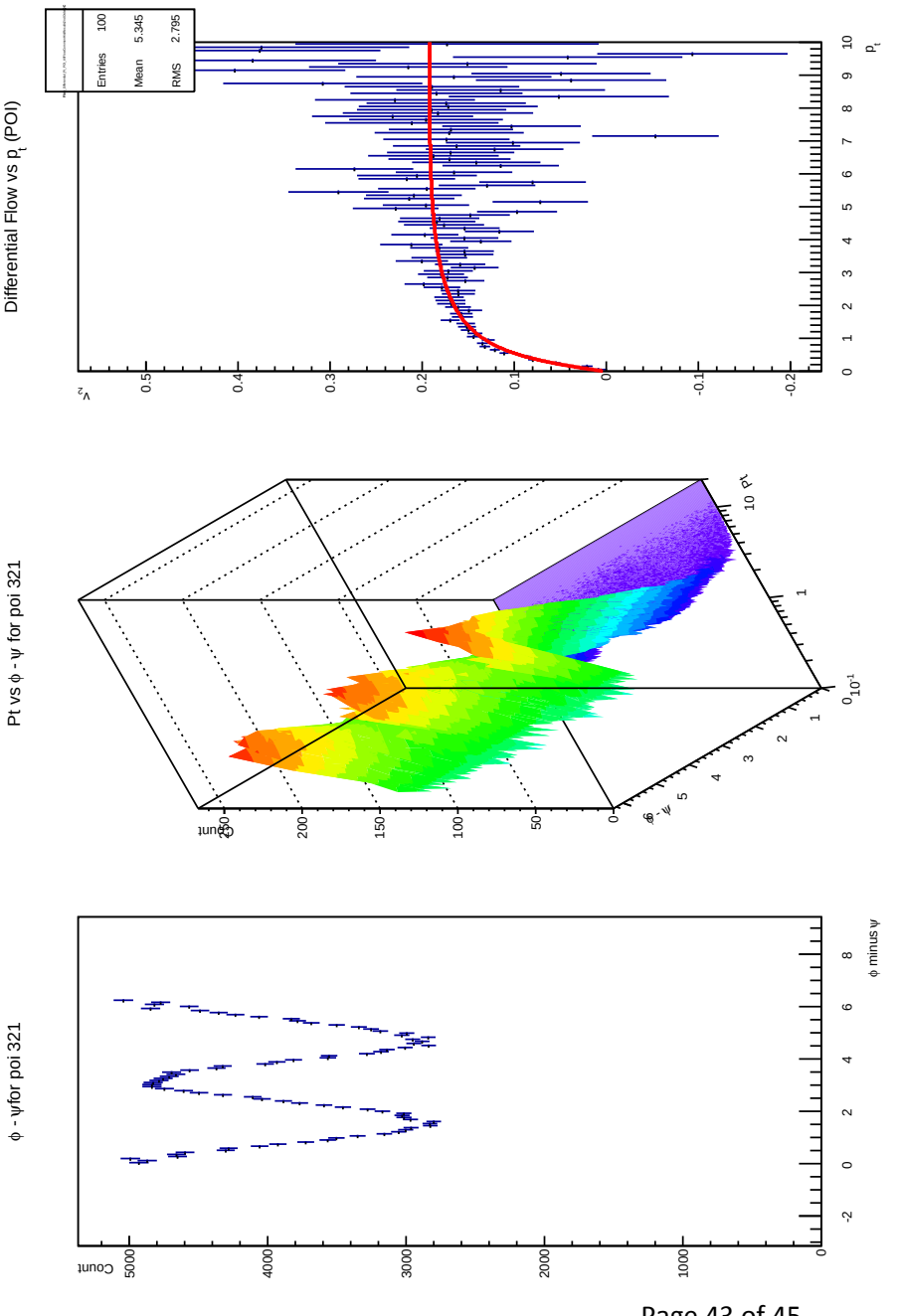

Appendix Figure 13

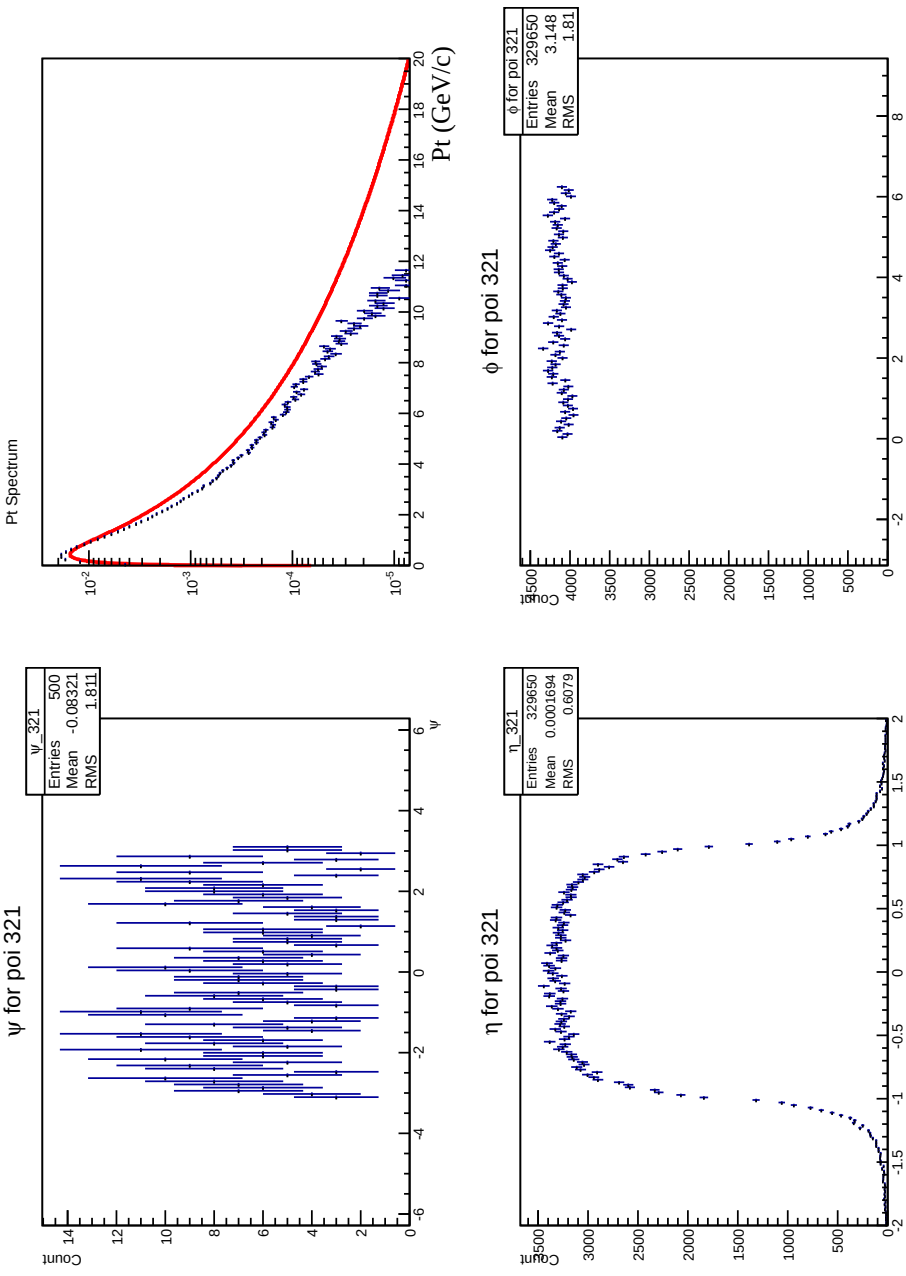

Appendix Figure 14